arXiv:1609.09470v1 [cs.SY] 29 Sep 2016

Macroscopic Modeling of Managed Lane-Freeway Networks

Matthew A. Wright, Gabriel Gomes, Roberto Horowitz, Alex A. Kurzhanskiy

September 30, 2016

Abstract

We propose a macroscopic modeling framework for networks of freeways equipped with managed lanes. Two types of managed lane configuration are considered: full-access, where vehicles can switch between the general purpose (GP) and the managed lanes anywhere; and *separated*, where such switching is allowed only at certain locations called *gates*. The proposed framework is based on widely-used first-order kinematic wave theory. In this model, the GP and the managed lanes are modeled as parallel links connected by nodes, where certain type of traffic may switch between GP and managed lane links.

We incorporate two phenomena into our model that are particular to managed lane-freeway networks: the *inertia effect* and the *friction effect*. The inertia effect reflects drivers' inclination to stay in their lane as long as possible and switch only if this would obviously improve their travel condition. The friction effect reflects the empirically-observed driver fear of moving fast in a managed lane while traffic in the adjacent GP links moves slowly due to congestion.

Calibration of models of large road networks is difficult, as the dynamics depend on many parameters whose numbers grow with the network's size. We present an iterative learning-based approach to calibrating our model's physical and driver-behavioral parameters. Finally, our model and calibration methodology are demonstrated with case studies of simulations of two managed lane-equipped freeways in Southern California.

Keywords: macroscopic first order traffic model, first order node model, multi-commodity traffic, managed lanes, HOV lanes, dynamic traffic assignment, inertia effect, friction effect

1 Introduction

Traffic demand in the developed and developing worlds shows no sign of decreasing, and the resulting congestion remains a costly source of inefficiency in the built environment. One study (Lomax et al., 2015) estimated that, in 2014, delays due to congestion cost drivers 7 billion hours and $160B in the United States alone, leading to the burning of 3 billion extra gallons of fuel. The historical strategy for accommodating more demand has been construction of additional infrastructure, so in recent years planners have developed strategies to improve the performance of *existing* infrastructure, both through improved road operations and demand management, which seeks to lower the number of vehicles on the road (Kurzhanskiy and Varaiya, 2015). One such strategy that has been widely adopted in the United States and other developed countries is the creation of so-called *managed lanes* (Obenberger, 2004). Managed lanes are implemented on freeways by restricting the use of one or more lanes to certain vehicles. As an example, high-occupancy-vehicle (HOV) lanes are intended to incentivize carpooling, which reduces the total number of cars on the road as a demand management outcome (Chang et al., 2008).

In addition to demand management, managed lanes provide an opportunity for improved road operations through real-time, responsive traffic control. For example, tolled express lanes give drivers the opportunity

to pay a toll to drive parallel to the general-purpose lanes on a (presumably less-congested) express lane. Traffic management authorities here have an opportunity to adjust the toll amount in response to the real-time state of traffic on the network. The potential for managed lanes as instruments for reactive, real-time traffic operations–in addition to their demand-management purpose–has driven their adoption among transportation authorities (Kurzhanskiy and Varaiya, 2015).

However, implementing managed lanes on a freeway can create complex traffic dynamics. Even on a single long, straight road, the dynamics of traffic flow are complex and not fully understood. Adding managed lanes alongside the non-managed, general-purpose (GP) lanes in effect creates two parallel and distinct, but coupled, traffic flows on the same physical structure. When used as intended, managed lanes carry flows with different velocity-occupancy-spacing characteristics and vehicle-type (e.g., strictly HOVs) compositions than the freeway. When vehicles move between the two lane flows, complex phenomena that are unobserved in GP-only freeways can emerge (see e.g. Daganzo and Cassidy (2008); Liu et al. (2011); Jang and Cassidy (2012); Cassidy et al. (2015), and others).

Making better use of managed lanes requires an understanding of the macroscopic behavior they induce. One widely-used tool for understanding macroscopic traffic flow behavior is the macroscopic traffic flow model. A rich literature exists on macroscopic models for flows on long roads, and at junctions where those roads meet, but an extension to the parallel-flows situation created by placing a managed lane in parallel with a freeway (a "managed lane-freeway network") is not straightforward. Such a model should describe when vehicles enter or exit the managed lane, and capture the interactions caused by the two flows' proximity, such as the so-called "friction effect" (Liu et al., 2011; Jang and Cassidy, 2012).

This paper presents macroscopic flow modeling tools we have used for simulation of managed lane-freeway networks. We begin in Section 2 with a discussion of relevant modeling tools from the literature, and how we make use of them. Section 3 describes network structures for the two common managed lane configurations: gated-access and full-access (ungated) lanes. This Section also describes models for friction and inertia effects that arise in managed lanes. Section 4 describes calibration methodologies for both network configurations. Section 5 presents case studies of two networks, one each of gated- and full-access, and typical macroscopic simulation results. Finally, we present conclusions in Section 6.

2 Managed Lane Modeling

The modeling techniques presented in this paper are based in the first-order macroscopic traffic flow model. Macroscopic models are those traffic models that describe aggregate traffic flows as fluids following a one-dimensional conservation law. We briefly introduce our notation here, but do not discuss the basics of first-order models. Detailed reviews are available in many references.

2.1 Modeling basics

In a macroscopic simulation, a road is divided into discrete cells, which we refer to as *links*. Links are drawn between *nodes*: a link begins at one node and ends at another. Many links may begin and end at each node. Each link l has a occupancy n_l, which is the number of cars in the link. In a first-order model, the traffic flows are fully prescribed by the occupancy. From timestep t to $t+1$, link l's occupancy updates according to the equation

$$n_l(t+1) = n_l(t) + \sum_{i=1}^{M} f_{il}(t) - \sum_{j=1}^{N} f_{lj}(t), \tag{2.1}$$

where $f_{il}(t)$ is the flow (number of vehicles) leaving link i and entering link l at time t, $f_{lj}(t)$ is the flow leaving link l and entering link j at time t, M is the number of links that end at link l's beginning node, and N is the number of links that begin at link l's ending node.

Computing the inter-link flows f requires the use of two intermediate quantities for each link. These are the link demand $S_l(t)$, which is the number of vehicles that wish to exit link l at timestep t, and the link supply, $R_l(t)$, which is the number of vehicles for which link l has space for at time t. Both S_l and R_l are functions of the occupancy n_l. The model that computes S_l and R_l from n_l is often called the "fundamental diagram" or "link model," and the model that computes the flows f from all links' supplies and demands is called the "node model."

A brief outline of how first-order macroscopic simulation of a road network (sometimes called a "dynamic network loading" simulation) is performed is:

1. At time t, use the link model for each link l to compute the link's demand $S_l(t)$ and supply $R_l(t)$ as a function of its occupancy $n_l(t)$.
2. Use the node model for each node to compute the throughflows f_{ij} for all incoming links i and outgoing links j as functions of $S_i(t)$, $R_j(t)$, and information about vehicles' desired movements ij.
3. Update the state of each link using 2.1
4. Increment t and repeat until the desired simulation end time is reached.

The tools described in this paper are compatible with any such link model. We make use of a particular node model that we have studied in Wright et al. (2016a,b). An aspect of this node model of particular relevance to managed lane modeling is our "relaxed first-in-first-out (FIFO)" construction (Wright et al., 2016a). This is necessary for modeling the flows between the GP and managed lanes. Without a FIFO relaxation, congestion in one of the two lane groups could block traffic in the other when that may be unrealistic (see Wright et al. (2016a, Section 2.2) for a detailed discussion).

So far, we have presented ingredients for a model that, while able to express many simple network topologies by joining links and nodes, does not capture several important behaviors in managed lane-freeway networks.

2.2 Multiple classes of vehicles and drivers

In (2.1), we describe the number of vehicles in a link as a single number, n_l. In this formulation, all vehicles are treated the same. However, for simulation in a managed lane-freeway network, it makes sense to break n_l into different classes of vehicles and/or drivers. For example, for a freeway with an HOV lane facility, we might consider two classes: HOVs and non-HOVs. To this end, (2.1) can be rewritten as

$$n_l^c(t+1) = n_l^c(t) + \sum_{i=1}^{M} f_{il}^c(t) - \sum_{j=1}^{N} f_{lj}^c(t), \tag{2.2}$$

where $c \in \{1, \ldots, C\}$ indexes vehicle classes (sometimes called "commodities" in the traffic literature).

Extending the occupancy update equation to multiple classes means that the link and node models must also be extended to produce per-class flows f_{ij}^c. In this paper, we will not specify a particular link model, but assume use of one that produces per-class demands S_i^c and overall supplies R_j. Examples of this type of link model include those considered in Wong and Wong (2002), Daganzo (2002), and van Lint et al. (2008) (examples of multi-class link models of second- or higher-order include those of Hoogendoorn and Bovy (2000), . These types of models have higher-order analogs of supply and demand). We use a particular node model that takes S_i^c and R_j to compute the flows f_{ij}^c.

2.3 Toplogical expression of managed lane-freeway networks

In both (2.1) and (2.2), we describe a link in terms of its total occupancy n_l. By discretizing the road into these one-dimensional links, we lose information about differences between vehicle proportions across lanes, as well as inter-lane and lane-changing behavior. This becomes a problem if this unmodeled behavior is of interest. In our setting, this means that modeling a freeway with a managed lane should not be done with a single link following (2.1) or (2.2), as it would be impossible to study the managed lane-freeway network behavior of interest.

Modeling differences in vehicle occupancy across lanes is natural in microscopic and mesoscopic (see, for example, Treiber et al. (1999); Hoogendoorn and Bovy (1999); Ngoduy (2006), and others) models, but macroscopic models, in their simplicity, have less readily-accessible avenues for including these differences. One straightforward method is to model each lane as a separate link, as in, e.g. Shiomi et al. (2015). However, this method has a few drawbacks. First, it requires the addition of some lane-assignment method to prescribe the proportions of each vehicle class c for each lane (such as a logit model as used in Farhi et al. (2013) and Shiomi et al. (2015)), which requires not-always-accessible data for calibration. Second, drastically increasing the number of links in a macroscopic model will necessarily increase the size of the state space and model complexity, which is, in a sense, incompatible with the overall goal of selecting a macroscopic model over a micro- or mesoscopic model: some of the "macro" in the macroscopic model is lost.

Instead, in this paper we choose to model the GP lanes (or "GP lane group") as one link and the parallel managed lanes (or "managed lane group") as another link. Applied to an entire length of road, this creates a network topology of two "parallel chains" of links - one GP and one managed. The two chains will share nodes, but cross-flows between the chains are permitted only in locations where there is physical access (i.e., no physical barriers) and policy access (i.e., no double-striped lines under U.S. traffic markings). Where cross-flows are possible, we do not use a logit model, but instead a driver behavior model first introduced in Wright et al. (2016a). This model is similar to the one described in Liu et al. (2012), though in this reference, GP-managed lane crossflows were not considered.

2.4 Observed phenomena in managed lane-freeway networks

The above-mentioned friction effect is one of several emergent behaviors thought to be important for understanding traffic phenomena present on managed lane-freeway networks, and has been blamed for some of the "underperformance" of managed lanes (Jang and Cassidy, 2012). To expand on our earlier description, the friction effect describes a tendency of vehicles in an HOV lane to reduce their speed when the vehicles in the adjacent GP lane(s) congest to the point where they slow down. It has been hypothesized that this occurs due to HOV drivers being uncomfortable at traveling at a drastically higher speed than the adjacent GP vehicles (Jang and Cassidy, 2012).

In Liu et al. (2012), the authors created a macroscopic model of a managed lane-freeway network with a friction effect model. They proposed modeling the friction effect by having two separate link models for the managed lanes – one each for when the GP lane is above or below some threshold density value.

In Section 3, we propose a more expressive model of the friction effect by replacing this piecewise implementation with a linear implementation, where the reduction in demands S_l^c in the managed lane is proportional to the speed differential between the managed lane(s) and GP lane(s). A linear relationship like this was hypothesized in e.g. Jang and Cassidy (2012, Fig. 5(c)). The magnitude of the friction effect (i.e., the degree to which managed lane drivers slow down to match GP lane drivers' speed) is thought to be dependent on the type of separation between the managed lane(s) and GP lane(s) (e.g., painted lines vs. a concrete barrier) (Jang et al., 2012), which can be encoded by selecting the linear coefficient to this speed differential.

3 Full- and Gated-Access Managed Lane-Freeway Network Topologies

We will consider two types of managed lane-freeway network configurations: *full access* and *separated with gated access*. In a a full-access configuration, the managed lane(s) are not physically separated from the GP lane(s), and eligible vehicles may switch between the two lane groups at any location. Often, full-access managed lane(s) are special-use only during certain periods of the day, and at other times they serve as GP lane(s) (e.g., HOV lanes are often accessible to non-HOVs outside of rush hour). On the other hand, in a gated-access configuration, traffic from may travel between the managed lane(s) and GP lane(s) only at certain locations, called *gates*; at non-gate locations, the two lane groups are separated by road markings (i.e., a double solid line in the U.S.) or a physical barrier. Usually, gated-access managed lanes are special-use at all times. The implemented managed lane access scheme depends on jurisdiction. For example, full-access lanes are common in Northern California, and separated lanes are common in Southern California.

The differences in physical geometry and access points between the two access types requires two different types of topology in constructing a network for a macroscopic model.

3.1 Note on link and node models used in this section

As discussed in the previous Section, we attempt to be agnostic with regards to the particular link model (e.g., first-order fundamental diagram) used in our implementations. However, in our model of the friction effect in Section 3.3, we parameterize friction being in effect on a particular link l for a particular vehicle class c at time t by adjusting that link's demand $S_l(t)$. For that discussion only, we specify a particular link model. This link model is discussed in Appendix A. This link model is also the one used in the simulations presented in Section 5.

The node model used here and for the remainder of this paper, when a particular form is necessary, is the one discussed in Wright et al. (2016a) and Wright et al. (2016b). We use this node model because it has a relaxation of the "conservation of turning ratios" or "first-in-first-out" (FIFO) constraint of most node models. This allows us to describe a set of GP lanes just upstream of an offramp with one link, and handle a condition of a congested offramp by having the congestion spill back onto only the offramp-serving lanes of the GP link (as opposed to the entirety of the GP link). See Wright et al. (2016a, Section 3) and Wright et al. (2016b) for more discussion.

3.2 Full-access Managed Lanes

A full-access managed lane configuration is presented in Figure 1: GP and managed links (recall, as discussed above, all GP lanes and all managed lanes are collapsed into one link each) are parallel with the same geometry and share the same begin and end node pairs; traffic flow exchange between GP and managed lanes can happen at every node. Note that in Figure 1, we use a slightly irregular numbering scheme so that it is clear whether a link is a GP link, managed lane link, or ramp link. Parallel links in the graph have numbers made up of the digit of their terminating node, with GP links having one digit (i.e., link 1), managed lane links having two (i.e., link 11), and ramp links having three (i.e., link 111). Note also that we use a U.S.-style, driving-on-the-right convention here, with the managed lane(s) on the left of the GP lanes and the ramps on the far right.

Links that are too long for modeling purposes (i.e., that create too low-resolution a model) may be broken up into smaller ones by creating more nodes, such as nodes 2 and 3 in Figure 1. Fundamental diagrams for parallel GP and HOV links may be different (Liu et al., 2011).

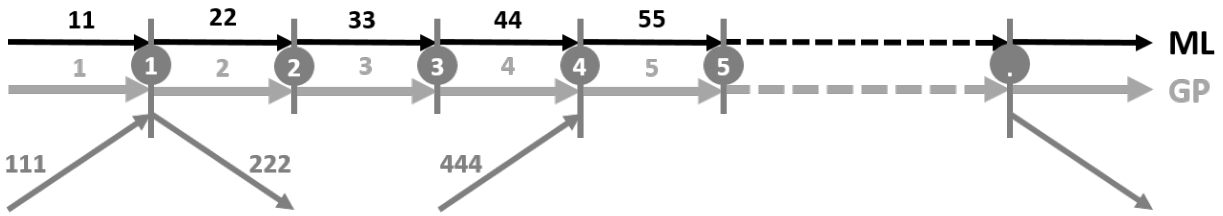

Figure 1: Freeway with full-access managed lane. ML = Managed Lane.

We introduce two vehicle classes ($C = 2$): $c = 1$ corresponds to the GP-only traffic and $c = 2$ corresponds to the special traffic. When the managed lane(s) is (are) active, $c = 1$-traffic is confined to the GP link, whereas $c = 2$-traffic can use both the GP and HOV links. We denote the portion of vehicles of class c in link i that will attempt to enter link j as $\beta^c_{i,j}$. This quantity is called the split ratio.

3.2.1 Split ratios for full-access managed lanes

We make an assumption that both vehicle classes take offramps at the same rate. For example, for node 1 in Figure 1, we might say that $\beta^1_{i,222} = \beta^2_{i,222} \triangleq \beta_{i,222}$. Strictly speaking, it is not is not necessary to assume that the $\beta^c_{i,222}$ are equal for all c. However, in practice the offramp split ratios are typically estimated from flow count data taken from detectors on the offramp and freeway. Generally speaking, these detectors cannot identify vehicle type, so the only quantity estimable is a flow-weighted average of the quantities $\beta^c_{i,222}$. To estimate the class-specific split ratios, one needs some extra knowledge of the tendency of each class to take each offramp (for example, that GP-only vehicles are half as likely as special traffic to take a certain offramp). Assuming that each class exits the freeway at the same rate is a simple and reasonable-seeming assumption.

This same problem of unidentifiability from typical data appears in several other split ratios. First, it may not be possible to tell, of the vehicles taking an offramp link, came from the upstream GP, managed lane, or (if present) onramp link. In this case, some assumptions must then be made. Two different assumptions that may be reasonable are (1) that vehicles in each link i take the offramp at the same rate, or (2) that no vehicles from the managed lane(s) are able to cross the GP lanes to take the onramp at this node, and that no vehicles entering via the onramp, if one is present, exit via the offramp at the same node. Looking back at node 1 in Figure 1 again, assumption (1) would say the $\beta_{i,222}$ are equal for all i, and assumption (2) would say $\beta_{11,222} = \beta_{111,222} = 0$. The best assumption for each node will depend on the road geometry for that particular part of the road (how near the offramp is to any onramps, how many GP lanes a vehicle in a managed lane would have to cross, etc.).

Second, the crossflows between the GP and managed lane links will not be observable for all but the most highly-instrumented freeways. For nodes that do not have a detectors immediately upstream and downstream, the special traffic split ratios between the GP and managed lane links must come from some driver choice model.

Putting together these assumption and the special-traffic-only policy for the managed lane, we can summarize most of the necessary split ratios needed for computing flows in a node model. For example, for node 1 in

Figure 1,

$$\beta^1_{i,j} = \left\{ \begin{array}{l|lll} & \boldsymbol{j=2} & \boldsymbol{j=22} & \boldsymbol{j=222} \\ \hline \boldsymbol{i=1} & 1-\beta_{1,222} & 0 & \beta_{1,222} \\ \boldsymbol{i=11} & \text{n/a} & \text{n/a} & \text{n/a} \\ \boldsymbol{i=111} & 1-\beta_{111,222} & 0 & \beta_{111,222} \end{array} \right.$$

$$\beta^2_{i,j} = \left\{ \begin{array}{l|lll} & \boldsymbol{j=2} & \boldsymbol{j=22} & \boldsymbol{j=222} \\ \hline \boldsymbol{i=1} & - & - & \beta_{1,222} \\ \boldsymbol{i=11} & - & - & \beta_{11,222} \\ \boldsymbol{i=111} & - & - & \beta_{111,222} \end{array} \right.$$

where "n/a" means that the split ratios $\beta^1_{11,j}$ are not applicable, as there should be vehicles of class $c = 1$ in the managed lane. The split ratios marked with a dash are those above-mentioned flows that may be wholly unobservable and come from some driver choice model. Of course, whatever method is chosen to compute these unknown split ratios, we must have $\beta^2_{i,2} + \beta^2_{i,22} = 1 - \beta^2_{i,222}$.

Similarly, for node 2, which does not have an onramp or offramp,

$$\beta^1_{i,j} = \left\{ \begin{array}{l|ll} & \boldsymbol{j=3} & \boldsymbol{j=33} \\ \hline \boldsymbol{i=2} & 1 & 0 \\ \boldsymbol{i=22} & \text{n/a} & \text{n/a} \end{array} \right.$$

$$\beta^2_{i,j} = \left\{ \begin{array}{l|ll} & \boldsymbol{j=3} & \boldsymbol{j=33} \\ \hline \boldsymbol{i=2} & - & - \\ \boldsymbol{i=22} & - & - \end{array} \right.$$

with "n/a" and the dash meaning the same as above.

As previously mentioned, full-access managed lanes often have certain time periods during which nonspecial ($c = 1$) traffic is allowed into the managed lane. We can model this change in policy simply by changing the split ratios at the nodes. For node 1, for example, the nonrestrictive policy is encoded as

$$\beta^c_{i,j} = \left\{ \begin{array}{l|lll} & \boldsymbol{j=2} & \boldsymbol{j=22} & \boldsymbol{j=222} \\ \hline \boldsymbol{i=1} & - & - & \beta_{1,222} \\ \boldsymbol{i=11} & - & - & \beta_{11,222} \\ \boldsymbol{i=111} & - & - & \beta_{111,222} \end{array} \right. \qquad \text{for } c = \{1, 2\},$$

and for node 2 as

$$\beta^c_{i,j} = \left\{ \begin{array}{l|ll} & \boldsymbol{j=3} & \boldsymbol{j=33} \\ \hline \boldsymbol{i=2} & - & - \\ \boldsymbol{i=22} & - & - \end{array} \right. \qquad \text{for } c = \{1, 2\}.$$

In other words, the managed lane link is treated as just more GP lane(s), and the split ratios governing the crossflows between the two links should be fond from some lane choice or driver choice model for both vehicle classes.

3.2.2 Node model for full-access managed lane-freeway networks

As mentioned in Section 3.1, we make use of a certain node model discussed in Wright et al. (2016a) and Wright et al. (2016b) for these models of managed lane-freeway networks. As mentioned above, this node model differentiates itself from others in that it has a relaxation of the common FIFO constraint. As an example, say that some link i has vehicles that wish to enter both links j andj'. If link j' is jammed and cannot accept any more vehicles, a strict FIFO constraint would say that the vehicles in i that wish to enter j' will queue at i's exit, and block the vehicles that wish to enter j. In a multi-lane road, however, only

certain lanes may queue, and traffic to j may still pass through other lanes. The relaxation is encoded in so-called "mutual restriction intervals" $\boldsymbol{\eta}^i_{j',j} \subseteq [0,1]$. This interval partly describes the overlapping regions of link i's exit that serve both links j and j'. For $\boldsymbol{\eta}^i_{j',j} = [y,z]$, a $z-y$ portion of i's lanes that serve j also serve j', and will be blocked by the cars queueing to enter j' when j' is congested. For example, if j is served by three lanes of i, and of those three lanes, the leftmost also serves j', we would have $\boldsymbol{\eta}^i_{j',j} = [0, 1/3]$.

As an example, we consider again node 1 in Figure 1. Say that the GP links (1 and 2) have four lanes, that the managed lane links (11 and 22) have two lanes, and that the onramp merges into and the offramp diverges from the rightmost GP lane. Further, we say that when the managed lane link is congested, vehicles in the GP lanes that wish to enter the managed lanes will queue only in the leftmost GP lane. On the other hand, when the GP link is congested, vehicles in the managed lanes that wish to enter the GP lanes will queue only in the rightmost managed lane. Finally, we suppose that a queue on the offramp (222) will cause vehicles to queue only on the rightmost GP lane. Taking together all of these statements, our mutual restriction intervals for this example are

$$\boldsymbol{\eta}^1_{j',j} = \begin{cases} & \boldsymbol{j=2} & \boldsymbol{j=22} & \boldsymbol{j=222} \\ \boldsymbol{j'=2} & [0,1] & [0,1] & [0,1] \\ \boldsymbol{j'=22} & [0,1/4] & [0,1] & \emptyset \\ \boldsymbol{j'=222} & [3/4,1] & \emptyset & [0,1] \end{cases}$$

$$\boldsymbol{\eta}^{11}_{j',j} = \begin{cases} & \boldsymbol{j=2} & \boldsymbol{j=22} & \boldsymbol{j=222} \\ \boldsymbol{j'=2} & [0,1] & [0,1/2] & \emptyset \\ \boldsymbol{j'=22} & [0,1] & [0,1] & \emptyset \\ \boldsymbol{j'=222} & \emptyset & \emptyset & [0,1] \end{cases}$$

$$\boldsymbol{\eta}^{111}_{j',j} = \begin{cases} & \boldsymbol{j=2} & \boldsymbol{j=22} & \boldsymbol{j=222} \\ \boldsymbol{j'=2} & [0,1] & [0,1] & [0,1] \\ \boldsymbol{j'=22} & \emptyset & [0,1] & \emptyset \\ \boldsymbol{j'=222} & [0,1] & [0,1] & [0,1] \end{cases}.$$

To read the above tables, recall that as written, j' is the congested, restricting link and j is the restricted link. These chosen restriction intervals allow for expected behavior in this network, such as a congested GP link causing possible queueing in the right managed lane (if some drivers are trying to enter the GP link), but no spillback into the left managed lane.

3.3 Friction Effect

The *friction effect* is an empirically-observed phenomenon where, in situations where managed lanes are relatively uncongested, the managed-lane traffic will still slow down when the adjacent GP lanes congest and slow down (see Daganzo and Cassidy (2008), Liu et al. (2011), Cassidy et al. (2015), etc.). It has been hypothesized (Jang and Cassidy, 2012) that this phenomenon arises from from the managed-lane drivers' fear that slower-moving vehicles will suddenly and dangerously change into the managed lane ahead of them.

We suggest modeling the friction effect based on a *feedback mechanism* that uses the difference of speeds in the parallel GP and managed lane links to scale down the flow (and therefore the speed) out of the managed lane link if necessary.

To explain the concept, we again refer to Figure 1 and consider parallel links 1 (GP) and 11 (managed lane). Recall that, under a first-order model (2.2), the speed of traffic in link l at time t is

$$v_l(t) = \begin{cases} \frac{\sum_{c=1}^{C}\sum_{j=1}^{N} f^c_{lj}(t)}{\sum_{c=1} n^c_l(t)} & \text{if } \sum_{c=1}^{c} n^c_l(t), \\ v^f_l(t) & \text{otherwise,} \end{cases} \tag{3.1}$$

where $v^f_l(t)$ is the theoretical freeflow speed of link l.

We say that the friction effect is present in managed lane link 11 at time t if

$$v_1(t-1) < \min\left\{v_1^f,\ v_{11}(t-1)\right\}, \tag{3.2}$$

which means that (1) the GP link is in congestion (its speed is below current free flow speed), and (2) the speed in the GP link is less than the speed in the HOV link. We denote this speed differential as

$$\Delta_{11}(t) = v_{11}^f - v_1(t-1). \tag{3.3}$$

It has been observed (Jang et al., 2012) that the magnitude of the friction effect – the degree to which managed-lane drivers slow down towards the GP lane's traffic speed – depends on the physical configuration of the road. For example, less of a friction effect will be present on managed lanes that are separated from the GP lanes by a buffer zone than those that are contiguous with the GP lanes (Jang et al., 2012), and the presence of a concrete barrier in a gated-access managed lane would reduce the magnitude of the friction effect further still. Other factors that may affect this magnitude include, for example, whether there is more than one managed lane, or whether there is a shoulder lane to the left of the managed lane that drivers could swerve into if necessary.

To encode this variability in the magnitude of the friction effect in managed lane link 11, we introduce $\sigma_{11} \in [0,1]$ the *friction coefficient* of this link. The friction coefficient reflects the strength of the friction. Its value depends on the particular managed configuration and is chosen by the modeler. A value of $\sigma_{11} = 0$ means there is no friction (which may be appropriate if, perhaps, the managed lane(s) are separated from the GP lanes by a concrete barrier), and $\sigma_{11} = 1$ means that the HOV link speed tracks the GP link speed exactly.

When the friction effect is active (i.e., when (3.2) is true), we adjust the fundamental diagram of the managed lane link by scaling down its theoretical freeflow speed $v_l^f(t)$, and propagate that change through the rest of the fundamental diagram parameters. The exact mathematical changes will of course be different for every different form of fundamental diagram. For the particular fundamental diagram discussed in Appendix A, this means adjusting the free flow speed and capacity as follows:

$$\hat{v}_{11}(t) = v_{11}^f(t) - \sigma_{11}\Delta_{11}(t); \tag{3.4}$$

$$\hat{F}_{11}(t) = \hat{v}_{11}(t) n_{11}^+, \tag{3.5}$$

and using these adjusted values in the calculation of the sending function (A.1),

$$S_{11}^c(t) = \hat{v}_{11}(t) n_{11}^c(t) \min\left\{1, \frac{\hat{F}_{11}(t)}{\hat{v}_{11}(t)\sum_{c=1}^{C} n_{11}^c(t)}\right\}. \tag{3.6}$$

For the fundamental diagram of Appendix A, we must also check whether

$$\sum_{c=1}^{C} n_l^c(t) < \frac{\hat{F}_{11}(t)}{v_{11}^f - \Delta_{11}(t)} = \frac{\hat{v}_{11}(t) n_{11}^+(t)}{v_{11}^f - \Delta_{11}(t)}. \tag{3.7}$$

If not, then applying friction will lead to the managed lane link speed falling below the GP link speed, and the unadjusted sending function should be used (the possibility of this happening is due to the use of two critical densities to create the fundamental diagram's "backwards lambda" shape).

Evidence of a friction effect reducing managed lane speed in a form that is linear in the speed differential (i.e., (3.4)) can be found in e.g., Jang et al. (2012). Again, the exact form of (3.6), the sending function with friction, will depend on the link's original fundamental diagram model.

3.4 Separated Managed Lanes with Gated Access

A separated, gated-access managed lane configuration is presented in Figure 2. Unlike the full-access configuration, the GP and managed lane link chains do not meet at every node. Instead, they need only meet at a few locations, which are the locations at which vehicles can move into and out of the managed lane(s). Note that, unlike the full-access configuration, there is no need for adjacent GP and managed lane links to be the same length.

As labeled in Figure 2, the nodes that the two link chains meet are called *gates* (as an aside, one way to describe the full-access managed lane configuration would be that every node is a gate). Similar to our construction of excluding GP-only traffic from the managed lane in the full-access case, We can disable flow exchange at a given gate by fixing split ratios so that they keep traffic in their link. For example, to disable the gate (the flow exchange between the two lanes) at node 2 in Figure 1, we set $\beta^c_{2,3} = 1$ and $\beta^c_{22,33} = 1$ ($\beta^c_{2,33} = 0$ and $\beta^c_{22,3} = 0$), $c = 1, 2$. Thus, the full access HOV lane can be easily converted into the separated HOV lane by setting non-exchanging split ratios everywhere but designated gate-nodes.

In practice, a gate is stretch of freeway may be a few hundreds of meters long (Cassidy et al., 2015), and, potentially, we can designate two or three nodes in a row as gates. In this paper, however, we model a gate as a single node.

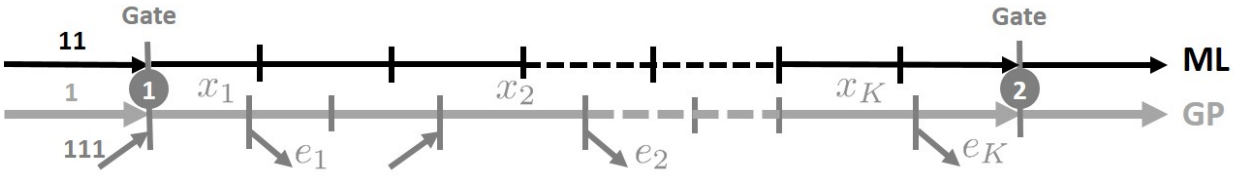

Figure 2: Freeway with separated managad lane and gates. ML = Managed Lane.

For the gated-access configuration, we suggest setting mutual restriction coefficients in the same manner as full-access managed lanes, in Section 3.2.2.

Compared to the full-access managed lane configuration,the gated-access configuration has a smaller friction effect (Jang et al., 2012): drivers in the separated HOV lane feel somewhat protected by the buffer, whether it is virtual (double solid line) or real (concrete), from vehicles changing abruptly from the slow moving GP lane and, therefore, do not drop speed as dramatically. The degree to which the friction effect is mitigated is disputed (see for example Footnote 3 in Cassidy et al. (2015)), but overall the bottlenecks created by the gates are much greater instigators of congestion (Cassidy et al., 2015). Inclusion of the friction effect in modeling separated managed lane configurations is thus not as essential as in modeling the full-access case.

3.4.1 Modeling a flow of vehicles from the managed lanes to the offramps

Recall from Section 3.2.1 that, in the full-access managed lane model, we can model vehicles moving from the managed lane link to offramps in a straightforward manner, by setting corresponding split ratios (for example, $\beta^c_{11,222}$, $c = 1, 2$, for node 1 in configuration from Figure 1). For the gated-access configuration, however, modeling traffic as moving from the managed lanes to offramps is more complicated: generally, gates do not coincide with off-ramp locations. In fact, there are typically between two and five offramps between two gate locations. We denote the offramps in the GP road segment connecting two gates as exits $e_1, e_2, \ldots, e_K$ (see Figure 2). These offramps cannot be accessed directly from the HOV lane. Instead, vehicles traveling in the managed lane link that intend to take one of the exits $e_1, \ldots, e_K$, must switch from

the managed lane link to the GP link at gate-node 1 and then be directed to the correct off-ramp. Creating a simulation where vehicles behave like this requires a more involved modeling construction.

To resolve this challenge, our gated-access model introduces new vehicle classes in addition to the $c = 1$ (GP-only) and $c = 2$ (special traffic) used in the full-access model of Section 3.2. These additional classes will be used to distinguish special traffic by its destination off-ramp. If K is the largest number of offramps between two adjacent gates, then altogether we have $C = K + 2$ classes: $c = 1, 2, e_1, \ldots, e_K$, where e_k indicates the class of vehicles that will exit through the kth offramp after leaving the managed lane through the gate. By definition, traffic of type $c = e_k$ *may* exist in the GP lane segment between gate 1 and off-ramp e_k, but there is *no traffic of this type* either in the GP link segment between offramp e_k and gate 2 or in the managed lane link. This movement pattern is ensured by setting *constant* split ratios:

$$\begin{array}{lll} \beta^{e_k}_{i\,x_1} = 1, \quad i = 1, 11, 111, & \text{direct all } e_k\text{-type traffic to the GP link at gate 1;} & \\ \beta^{e_k}_{x_k e_k} = 1, & \text{direct all } e_k\text{-type traffic to off-ramp } e_k; & (3.8) \\ \beta^{e_k}_{x_{k'} e_{k'}} = 0, \quad k' \neq k, & \text{do not send any } e_k\text{-type traffic to other off-ramps,} & \end{array}$$

where $k = 1, \ldots, K$, and x_k denotes the input GP link for the node that has the output link e_k (see Figure 2).

Vehicles of class $c = e_k$ do not enter the network via onramps or the upstream boundary, but instead are converted from special $c = 2$ traffic as it leaves the managed lane(s) through the gate. We perform this conversion as part of the link model computation, such that the total demand for the switching link, $\sum_{c=1}^{C} S_l^c$ remains the same before and after the switch. The exact link on which this switching takes place is the managed lane link immediately upstream of the gate (e.g., link 11 in Figure 2).

We say that the amount of vehicles that should change from vehicle class $c = 2$ to vehicle class e_k at time t is (using link 11 as an example) $n^2_{11}(t)\beta^2_{x_k e_k}(t)v_{11}(t)$, where $v_{11}(t)$ is in units of vehicles per simulation timestep (this factor is included so that the switching done is proportional to link 11's outflow, rather than its occupancy), $\beta^2_{x_k e_k}(t)$ is the split ratio from x_k, the GP link immediately upstream of exit e_k, and the exit e_k at time t. This statement is based on the assumption that the vehicles in the managed lane link will exit the freeway through exit e_k at the same rate as special ($c = 2$) vehicles that happened to stay in the GP lanes. That is, if a $\beta^2_{x_k e_k}$ portion of $c = 2$ vehicles intend to leave the GP lanes through exit e_k, then a $\beta^2_{x_k e_k}$ portion of the $c = 2$ vehicles in the managed lane(s) will leave the managed lane link at the closest upstream gate and leave the network at exit e_k when they reach it. Note that if there are $K' < K$ offramps between two particular gates, then no vehicles should switch to type $c = e_k, k \in \{K' + 1, \ldots, K\}$ at the upstream gate, as they would have no ramp to exit through.

After the switches to $c = e_k$ class traffic have been done, there may be unresolved split ratios for both classes $c = 1$ and $c = 2$ at the gates (similar to the dashed split ratios in the tables in Section 3.2.1). These split ratios should be filled in with the same tools as those in Section **??**: some sort of driver lane choice behavior.

3.4.2 Inertia Effect

At the end of the previous section, we mentioned that some split ratios will likely be undefined after switching $c = 2$ class vehicles to the $c = e_k$ classes. In particular, $c = 2$ class vehicles in the upstream GP link (e.g., link 1 in Figure 2) and remaining $c = 2$ vehicles in the upstream managed lane link (e.g. link 11 in Figure 2) will need to decide whether to pass through the gate or remain in their current lane. Example tools for modeling driver lane choices such as these include the class of "logit" logistic regression models (McFadden, 1973), or dynamic route assignment models such as that presented in Wright et al. (2016a).

When applied to lane choice (as in, e.g., Farhi et al. (2013)), logit models produce a set of portions in $[0, 1]$, one for each lane, that sum to one. Each lane's value is the equilibrium portion of vehicles that will travel on that lane. In a dynamic simulation context, such as considered in this article, the differences between the logit model's equilibrium portions and the current distribution of vehicles across lanes at time t are used

to select split ratios at time t such that the actual distribution approaches the logit equilibrium. We argue, though, that use of this sort of split ratio solver in unmodified form might be inappropriate for computing gate split ratios in the gated-access managed lane configuration. Unmodified, a value function for either the GP or managed lane link might include terms such as the link's speed of traffic, occupancy, etc. However, often a gated-access managed lane is separated from the GP lanes by some buffer zone that or visibility-obstructing barrier that makes switching between the two links more hazardous than switching between two contiguous lanes. Therefore, it would be appropriate to modify the logit model's value function such that staying in the current link (e.g., the movements (1,2) and (11,22) in Figure 3) has some positive value for drivers, and the gains in, e.g., travel time for ingress/egress movements (e.g., (1,22) and (11,2) in Figure 3), must be of more value than the staying-in-the-lane value. We refer to this model as an *inertia effect*.

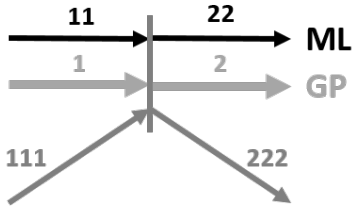

Figure 3: A node where some of the input links form travel facilities with some of the output links. ML = Managed Lane.

We may also incorporate an inertia effect into dynamic split ratio solvers such as the one introduced in Wright et al. (2016a). At time t This particular algorithm selects split ratios to attempt to balance the occupancy ratio at the next timestep $t+1$, $\sum_c n_l^c(t+1)/n_l^J$, where n_l^J is the jam occupancy, or the maximum number of vehicles that link l can hold. For example, if applied to the node in Figure 3, this algorithm would attempt to make $\sum_c n_2^c(t+1)/n_l^J$ and $\sum_c n_{22}^c(t+1)/n_l^J$ as equal as possible. For more details, see Wright et al. (2016a).

Here, we modify several steps of the solver so that this equality-seeking goal is balanced with a goal towards enforcing the inertia effect. We illustrate these changes with the particular example of the node in Figure 3. Ensuring that the split ratio assignment algorithm gives preferences to movements (1,2) and (11,22) over (1,22) and (11,2) can be done in step 5 of the original algorithm, setting of oriented priorities. Specifically, we modify (4.3) in Wright et al. (2016a). For this particular example, the original formula gives us:

$$\begin{array}{ll} \gamma_{1,2}^c(k) = \tilde{\beta}_{1,2}^c(k) + \frac{\overline{\beta}_1^c(k)}{2} & \gamma_{1,22}^c(k) = \tilde{\beta}_{1,22}^c(k) + \frac{\overline{\beta}_1^c(k)}{2}; \\ \gamma_{11,2}^c(k) = \tilde{\beta}_{11,2}^c(k) + \frac{\overline{\beta}_{11}^c(k)}{2} & \gamma_{11,22}^c(k) = \tilde{\beta}_{11,22}^c(k) + \frac{\overline{\beta}_{11}^c(k)}{2}. \end{array}$$

Since for $k=0$ $\tilde{\beta}_{i,j}^c(0)=0$, $i=1,11$, $j=2,22$, we get $\gamma_{1,2}^c(0) = \gamma_{1,22}^c(0) = \frac{\overline{\beta}_1^c(k)}{2}$ and $\gamma_{11,2}^c(0) = \gamma_{11,22}^c(0) = \frac{\overline{\beta}_{11}^c(k)}{2}$, which, according to (4.2) in Wright et al. (2016a), yields $\tilde{p}_{1,2}(0) = \tilde{p}_{1,22}(0)$ and $\tilde{p}_{11,2}(0) = \tilde{p}_{11,22}(0)$.

For each input link i that forms one lane with an output link $\hat{\jmath}$ and class c, such that $\hat{\jmath} \in V_i^c$, (4.3) in Wright et al. (2016a) can be modified as follows:

$$\gamma_{ij}^c(k) = \begin{cases} \beta_{ij}^c, & \text{if split ratio is defined a priori: } \{i,j,c\} \in \mathcal{B}, \\ \tilde{\beta}_{ij}^c(k) + \overline{\beta}_i^c(k)\lambda_i^c, & i \text{ and } j \text{ form one lane: } j = \hat{\jmath}, \\ \tilde{\beta}_{ij}^c(k) + \overline{\beta}_i^c(k)\frac{1-\lambda_i^c}{|V_i^c|-1}, & i \text{ and } j \text{ are in different lanes: } j \neq \hat{\jmath}, \end{cases} \tag{3.9}$$

where the parameter $\lambda_i^c \in \left[\frac{1}{|V_i^c|}, 1\right]$ is called the *inertia coefficient*, and indicates how strong the inertia effect is. With $\lambda_i^c = \frac{1}{|V_i^c|}$, (3.9) reduces to the original formula, (4.3) of Wright et al. (2016a). With $\lambda_i^c = 1$, all the *a priori* unassigned traffic from link i must stay in its lane — be directed to output link $\hat{\jmath}$. The choice of λ_i lies with the modeler. In the case of example from Figure 3, the modified formula (3.9) yields:

$$\begin{array}{ll} \gamma_{1,2}^c(k) = \tilde{\beta}_{1,2}^c(k) + \overline{\beta}_1^c(k)\lambda_1^c & \gamma_{1,22}^c(k) = \tilde{\beta}_{1,22}^c(k) + \overline{\beta}_1^c(k)(1-\lambda_1^c); \\ \gamma_{11,2}^c(k) = \tilde{\beta}_{11,2}^c(k) + \overline{\beta}_{11}^c(k)(1-\lambda_{11}^c) & \gamma_{11,22}^c(k) = \tilde{\beta}_{11,22}^c(k) + \overline{\beta}_{11}^c(k)\lambda_{11}^c, \end{array} \tag{3.10}$$

where $\lambda_1, \lambda_{11} \in \left[\frac{1}{2}, 1\right]$, and picking $\lambda_1 > \frac{1}{2}$ ($\lambda_{11} > \frac{1}{2}$) would give preference to movement (1,2) over (1,22) (and (11,22) over (11,2)).

The way of choosing λ_i^c for multiple input links is not obvious and an arbitrary choice may result in an unbalanced flow distribution among output links. Therefore, we suggest picking just one input-output pair $(\hat{\imath}, \hat{\jmath})$, and for that input link setting $\lambda_{\hat{\imath}}^c = 1$, while for other input links i setting $\lambda_i^c = \frac{1}{|V_i^c|}$, $c = 1, \ldots, C$. The input link $\hat{\imath}$ must be from the lane that is expected to have a positive net inflow of vehicles as a result of the resulting split ratios and flows computed by the node model. So,

$$\hat{\imath} = \arg\min_{i \in \hat{U}} = \frac{\sum_{c:\{i,j,c\} \in \overline{\mathcal{B}}} \overline{S}_i^c + \sum_{i:\{i,j,c\} \in \mathcal{B}} \sum_{c:\{i,j,c\} \in \mathcal{B}} \beta_{ij}^c S_i^c}{R_j}, \tag{3.11}$$

where

$$\hat{U} = \{\text{input links } i : \exists j, c, \text{ s.t. } j \in V_i^c \text{ and the pair of links } (i,j) \text{ belongs to the same lane}\}, \tag{3.12}$$

and j denotes the output link that is in the same lane as input link i.

For the particular example node in Figure 3, we need to determine whether flow from link 1 will proceed to link 2 or flow from link 11 to link 22, while other *a priori* undefined split ratios will be computed according to the split ratio assignment algorithm. If $\hat{\imath} = 11$, then $\lambda_{11} = 1$, $\lambda_1 = \frac{1}{2}$, and *a priori* unassigned traffic in the managed lane will stay in the managed lane ($\beta_{11,2}^c = 0$), while the *a priori* unassigned traffic coming from links 1 and 111, will be distributed between links 2 and 22 according to the dynamic split ratio solver.

On the other hand, if $\hat{\imath} = 1$, then $\lambda_1 = 1$, $\lambda_{11} = \frac{1}{2}$, and *a priori* unassigned traffic in the GP lane will stay in the GP lane ($\beta_{1,22}^c = 0$), while the a priori unassigned traffic coming from links 11 and 111, will be distributed between links 2 and 22 according to the dynamic split ratio solver.

4 Calibrating the Managed Lane-Freeway Network Model

When it comes to the simulation of real world traffic networks, in our case freeways with managed lanes, the quality of the simulation results is assessed by comparing them with detector measurements. In this Section, we present a methodology to calibrate a model to measurements consisting of flow and speed data on the freeway mainline (from both GP and managed lanes), as well as flow data on on- and offramps. To match the detector measurements, the simulation model's parameters need to be tuned. The tunable parameters of our model are:

- Fundamental diagram parameters, free flow speed v_l, congestion wave speed w_l, capacity F_l and the jam density n_l^J, for each link. Calibration of a fundamental diagram is typically agnostic to the node model and network topology, and there exists an abundant literature on this topic. For the purposes of the simulations in the following Section, we used the method of Dervisoglu et al. (2009), but any other method is appropriate.
- Percentage of special (able to access the managed lane) vehicles in the traffic flow entering the system. This parameter depends on, e.g., the time of day and location as well as on the type of managed lane. It could be roughly estimated as a ratio of the managed lane vehicle count to the total freeway vehicle count during periods of congestion at any given location.
- Inertia coefficients. These parameters affect only how traffic of different classes mixes in different links, but they have no effect on the total vehicle counts produced by the simulation. For setting the inertia coefficients, we suggest the approach described in the second part of the Section **??**.

- Friction coefficients. How to tune these parameters is an open question. In Jang and Cassidy (2012) the dependency of a managed lane's speed on the GP lane speed was investigated under different occupancies of the managed lane, and the presented data suggests that although the correlation between the two speeds exists, it is not overwhelmingly strong, below 0.4. Therefore, we suggest setting friction coefficients to values not exceeding 0.4.
- Mutual restriction intervals. It is also an open question how to estimate mutual restriction intervals from the measurement data. See the discussion in Section 3.2.2 for some guidelines.
- Off-ramp split ratios. The focus of this Section will be on computing these split ratios given known off-ramp flows.

4.1 Split Ratios for a Full-Access Managed Lane

Consider a node, one of whose output links is an offramp, as depicted in Figure 3. We shall make the following assumptions.

1. Total flow entering the offramp, $\hat{f}^{in}_{222}$, at any given time is known (from measurements) and is not restricted by the offramp supply: $\hat{f}^{in}_{222} < R_{222}$.
2. Portions of traffic sent to the offramp from the managed lane and from the GP lane at any given time are equal: $\beta^c_{1,222} = \beta^c_{11,222} = \beta$, $c = 1, \dots, C$.
3. None of the flow coming from the onramp (link 111), if such flow exists, is directed toward the offramp. In other words, $\beta^c_{111,222} = 0$, $c = 1, \dots, C$.
4. The distribution of flow portions not directed to the off-ramp between the managed lane and the GP output links is known. This can be written as: $\beta^c_{ij} = (1-\beta)\delta^c_{ij}$, where $\delta^c_{ij} \in [0,1]$, as well as $\beta_{111,j}$, $i = 1, 11$, $j = 2, 22$, $c = 1, \dots, C$, are known.
5. The demand S^c_i, $i = 1, 11, 111$, $c = 1, \dots, C$, and supply R_j, $j = 2, 22$, are given.

At any given time, β is unknown and is to be found.

If β were known, the node model would compute the input-output flows, in particular, $f_{i,222} = \sum_{c=1}^{C} f^c_{i,222}$, $i = 1, 11$. Define

$$\psi(\beta) = f_{1,222} + f_{11,222} - \hat{f}^{in}_{222}. \tag{4.1}$$

Our goal is to find β from the equation:

$$\psi(\beta) = 0, \tag{4.2}$$

such that $\beta \in \left[\frac{\hat{f}^{in}_{222}}{S_1+S_{11}}, 1\right]$, where $S_i = \sum_{c=1}^{C} S^c_i$. Obviously, if $S_1 + S_{11} < \hat{f}^{in}_{222}$, the solution does not exist, and the best we can do in this case, is to set $\beta = 1$ directing all traffic from links 1 and 11 to the off-ramp.

Suppose now that $S_1 + S_{11} >= \hat{f}^{in}_{222}$. For any given $\hat{f}^{in}_{222}$, we assume $\psi(\beta)$ is a monotonically increasing function of β (this assumption is true for the particular node model of Wright et al. (2016a). Moreover, $\psi\left(\frac{\hat{f}^{in}_{222}}{S_1+S_{11}}\right) \leq 0$, while $\psi(1) \geq 0$. Thus, the solution of (4.2) within given interval exists and can be obtained using the *bisection method*.

The algorithm for finding β follows.

1. Initialize:

$$\begin{aligned} \underline{b}(0) &:= \frac{\hat{f}_{222}^{in}}{S_1 + S_{11}}; \\ \overline{b}(0) &:= 1; \\ k &:= 0. \end{aligned}$$

2. If $S_1 + S_{11} \leq \hat{f}_{222}^{in}$, then set $\beta = 1$ and stop.

3. Use the node model with $\beta = \underline{b}(0)$ and evaluate $\psi(\beta)$. If $\psi(\underline{b}(0)) \geq 0$, then set $\beta = \underline{b}(0)$ and stop.

4. Use the node model with $\beta = \frac{\underline{b}(k)+\overline{b}(k)}{2}$ and evaluate $\psi(\beta)$. If $\psi\left(\frac{\underline{b}(k)+\overline{b}(k)}{2}\right) = 0$, then set $\beta = \frac{\underline{b}(k)+\overline{b}(k)}{2}$ and stop.

5. If $\psi\left(\frac{\underline{b}(k)+\overline{b}(k)}{2}\right) < 0$, then update:

$$\begin{aligned} \underline{b}(k+1) &= \frac{\underline{b}(k) + \overline{b}(k)}{2}; \\ \overline{b}(k+1) &= \overline{b}(k). \end{aligned}$$

   Else, update:

$$\begin{aligned} \underline{b}(k+1) &= \underline{b}(k); \\ \overline{b}(k+1) &= \frac{\underline{b}(k) + \overline{b}(k)}{2}. \end{aligned}$$

6. Set $k := k + 1$ and return to step 4.

4.2 Split Ratios for the Separated Managed Lane

The configuration of a node with an offramp as one of the output links is simpler in the case of a separated HOV lane, as shown in Figure 4. Here, traffic cannot directly go from the HOV lane to link 222, and, thus, we have to deal only with the 2-input-2-output node. There is a caveat, however. Recall from Section 3.4 that in the separate managed lane case we have destination-based traffic classes, and split ratios for destination-based traffic are fixed.

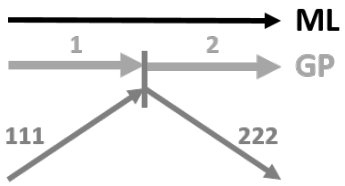

Figure 4: A node with a GP link and an on-ramp as inputs, and a GP link and an off-ramp as outputs.

We shall make the following assumptions:

1. Total flow entering the off-ramp, $\hat{f}_{222}^{in}$, at any given time is known (from measurements) and is not restricted by the off-ramp supply: $\hat{f}_{222}^{in} < R_{222}$.

2. All the flow coming from the on-ramp (link 111), if such flow exists, is directed toward the GP link 2. In other words, $\beta^c_{111,2} = 1$ and $\beta^c_{111,222} = 0$, $c = 1, \ldots, C$.

3. The demand S^c_i, $i = 1, 111$, $c = 1, \ldots, C$, and supply R_2 are given.

4. Denote the set of destination-based commodities as $\mathcal{D}$. Split ratios β^c_{1j} for $c \in \mathcal{D}$ are known. Split ratios $\beta^c_{1j} = \beta$ for $c \in \overline{\mathcal{D}}$, where β is to be determined.

The first three assumptions here reproduce assumptions 1, 3 and 5 made for the full-access managed lane case. Assumption 4 is a reminder that there is a portion of traffic flow that we cannot direct to or away from the off-ramp, but we have to account for it.

Similarly to the full-access managed lane case, define function $\psi(\beta)$:

$$\psi(\beta) = \sum_{c \in \overline{\mathcal{D}}} f^c_{1,222} + \sum_{c \in \mathcal{D}} f^c_{1,222} - \hat{f}^{in}_{222}, \tag{4.3}$$

where $f^c_{1,222}$, $c = 1, \ldots, C$ are determined by the node model from Section **??**. The first term of the right-hand sight of (4.3) depends on β. As before, we assume $\psi(\beta)$ is a monotonically increasing function. We look for the solution of equation (4.2) on the interval $[0, 1]$. This solution exists iff $\psi(0) \leq 0$ and $\psi(1) \geq 0$. The algorithm for finding β is the same as the one presented in the previous section, except that $\underline{b}(0)$ should be initialized to 0, and S_{11} is to be assumed 0.

4.3 The Iterative Calibration Process

The model calibration follows the workflow diagram shown in Figure 5.

1. We start by assembling the available measurement data. Fundamental diagrams are assumed to be given. Mainline and on-ramp demand is specified per 5-minute periods together with the special vehicle portion parameter indicating the fraction of the input demand that is able to access the managed lane. Initially, we do not know offramp split ratios as they cannot be measured directly. Instead, we use some arbitrary values to represent them and call these values "initially guessed offramp split ratios". Instead of the offramp split ratios, we have the flows directed to offramps, to which we refer to as *offramp demand*.

2. We run our network simulation for the entire simulation period, here in step 5 the *a priori* undefined split ratios between traffic in the GP and in the managed lanes are assigned using a split ratio solver.

3. Using these newly assigned split ratios we run the LNCTM model again, only this time, instead of using given offramp split ratios, we compute them from the given off-ramp demand as described in Sections 4.1 and 4.2. As a result of this step, we obtain new off-ramp split ratios.

4. Now we run the network simulation as we did originally, in step 2, only this time with new offramp split ratios, and record the simulation results — density, flow, speed, as well as performance measures such as vehicle miles traveled (VMT) and vehicle hours traveled (VHT).

5. Check if the resulting off-ramp flows match the off-ramp demand. If yes, proceed to step 6, otherwise, repeat steps 2-5. Usually, it takes the process described in steps 2-5 no more than two iterations to converge.

6. Evaluate the simulation results:

   - correctness of bottleneck locations and activation times;
   - correctness of congestion extension at each bottleneck;

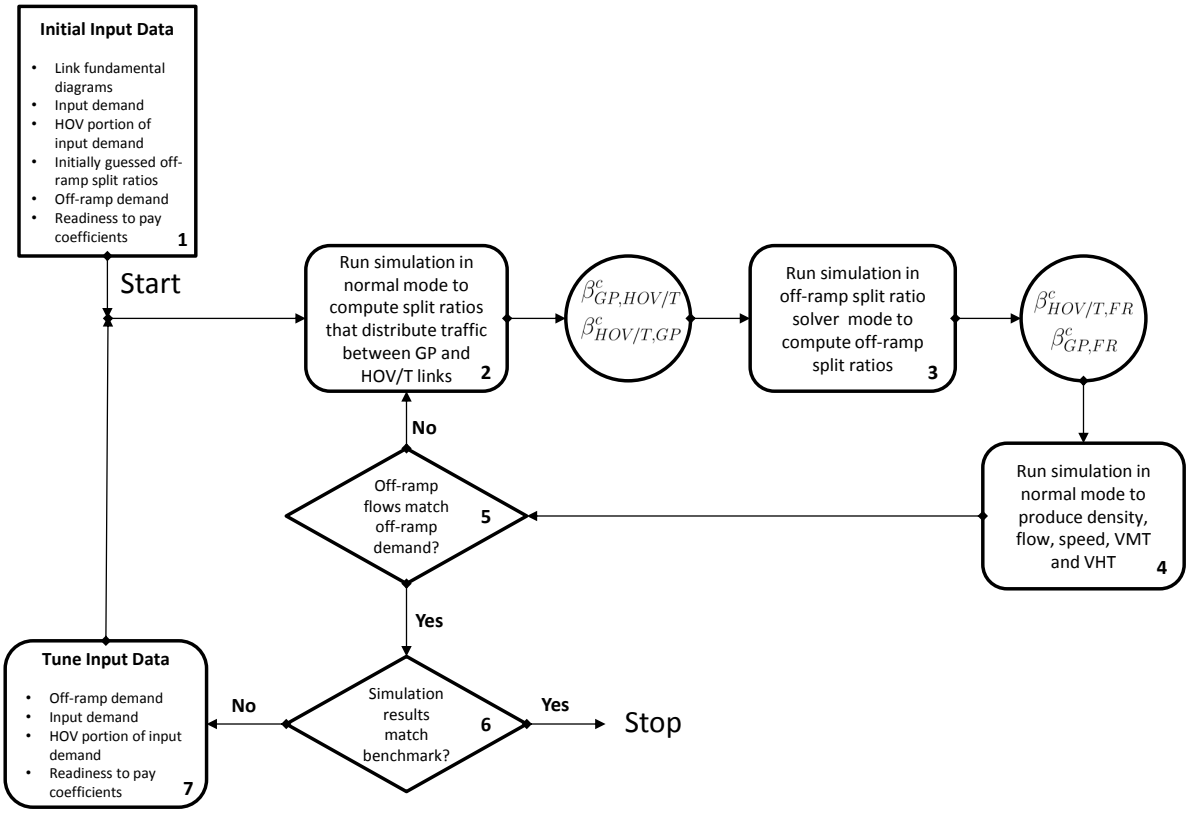

Figure 5: Calibration workflow.

- correctness of VMT and VHT.

If the simulation results are satisfactory, stop. Otherwise, proceed to step 7.

7. Tune input data in the order shown in block 7 of Figure 5.

5 Simulation Results

5.1 Full-Access Managed Lane Case Study: Interstate 680 North

We consider a 26.8-mile stretch of I-680 North freeway in Contra Costa County from postmile 30 to postmile 56.8, shown in Figure 6, as a test case for the full access managed lane configuration. This freeway's managed lane is a high-occupancy-vehicle (HOV) lane, which allows vehicles with two or more passengers. This stretch contains two HOV lane segments whose begin and end points are marked on the map. The first HOV segment is 12.3 miles long and will be converted to HOT in spring 2017 **?**, and the second HOV segment is 4.5 miles long. There are 26 on-ramps and 24 off-ramps. The HOV lane is active from 5 to 9 am and from 3 to 7 pm. The rest of the time the HOV lane behaves as a GP lane.

To build the model, we used data collected for the I-680 Corridor System Management Plan (CSMP) study **?**. The bottleneck locations as well as their activation times and congestion extension were identified in that

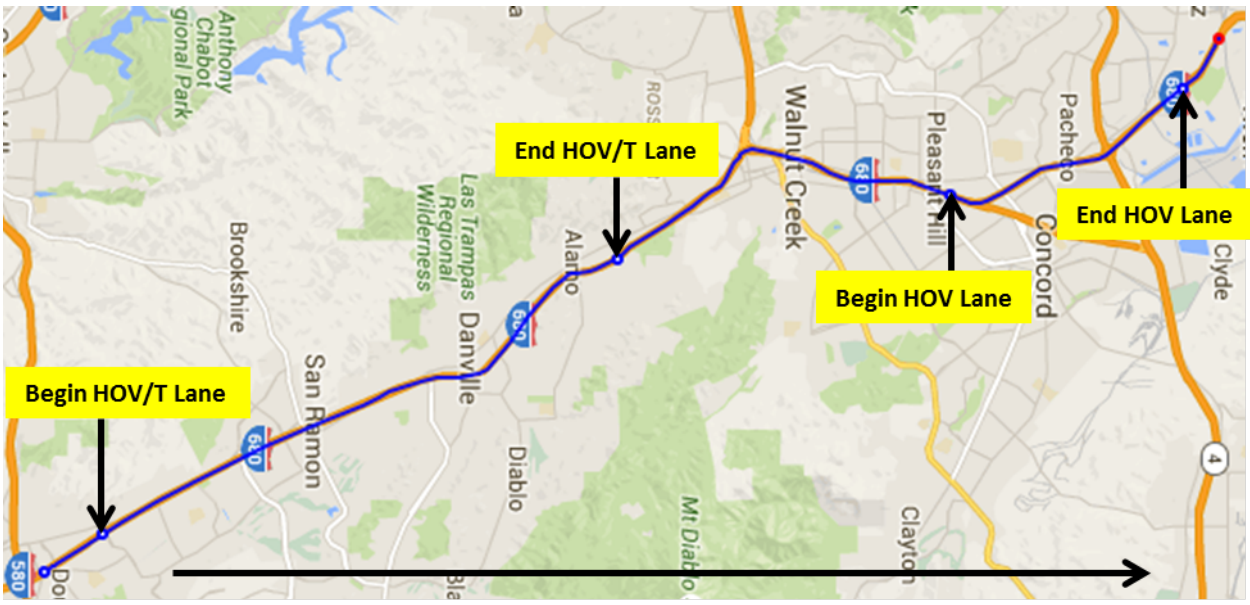

Figure 6: Map of I-680 North in Contra Costa County.

study using video monitoring and tachometer vehicle runs. On- and off-ramp flows were given in 5-minute increments. Here we assume that HOV portion of the input demand is 15%. The model was calibrated to a *typical weekday*, as suggested in the I-680 CSMP study.

Fundamental diagrams were assigned as follows:

- Capacity of the ordinary GP lane is 1,900 vphl;
- Capacity of the auxiliary GP lane is 1,900 vphl;
- Capacity of HOV lane is 1,800 vphl while active and 1,900 vphl when it behaves as a GP lane;
- Free flow speed varies between 63 and 70 mph — its measurements came partially from PeMS California Department of Tranportation and partially from tachometer vehicle runs.
- Congestion wave speed for each link was taken as 1/5 of the free flow speed.

The modeling results are presented in Figures 7, 8 and 9 showing speed, density and flow contours in the GP and the HOV lanes respectively. Each of these plots consists of the top, corresponding to the HOV lane, and bottom, corresponding to the GP lane, parts. In all the plots traffic moves from left to right along the "Absolute Postmile" axis, while the vertical axis represents time. Bottleneck locations and congestion areas identified by the I-680 CSMP study are marked by blue boxes in GP lane contours. HOV lane does not get congested, but there is a speed drop due to the *friction effect*. The friction effect, when vehicles in the HOV lane slow down because of the slow moving GP lane traffic, can be seen in the HOV lane speed contour in Figure 7.

Figure 10 shows an example of how well the off-ramp flow computed by the simulation matches the target, referred to as *off-ramp demand*, taken from the off-ramp at Crow Canyon Road. We can see that in the beginning and in the end of the day the computed flow falls below the target (corresponding areas are marked with red circles). This is due to the shortage of the mainline traffic — the off-ramp demand cannot be satisfied.

Finally, Table 1 summarizes the performance measurements — vehicle miles traveled (VMT), vehicle hours traveled (VHT) and delay in vehicle-hours — computed by simulation versus collected in the course of the I-680 CSMP study. Delay is computed for vehicles with speed below 45 mph.

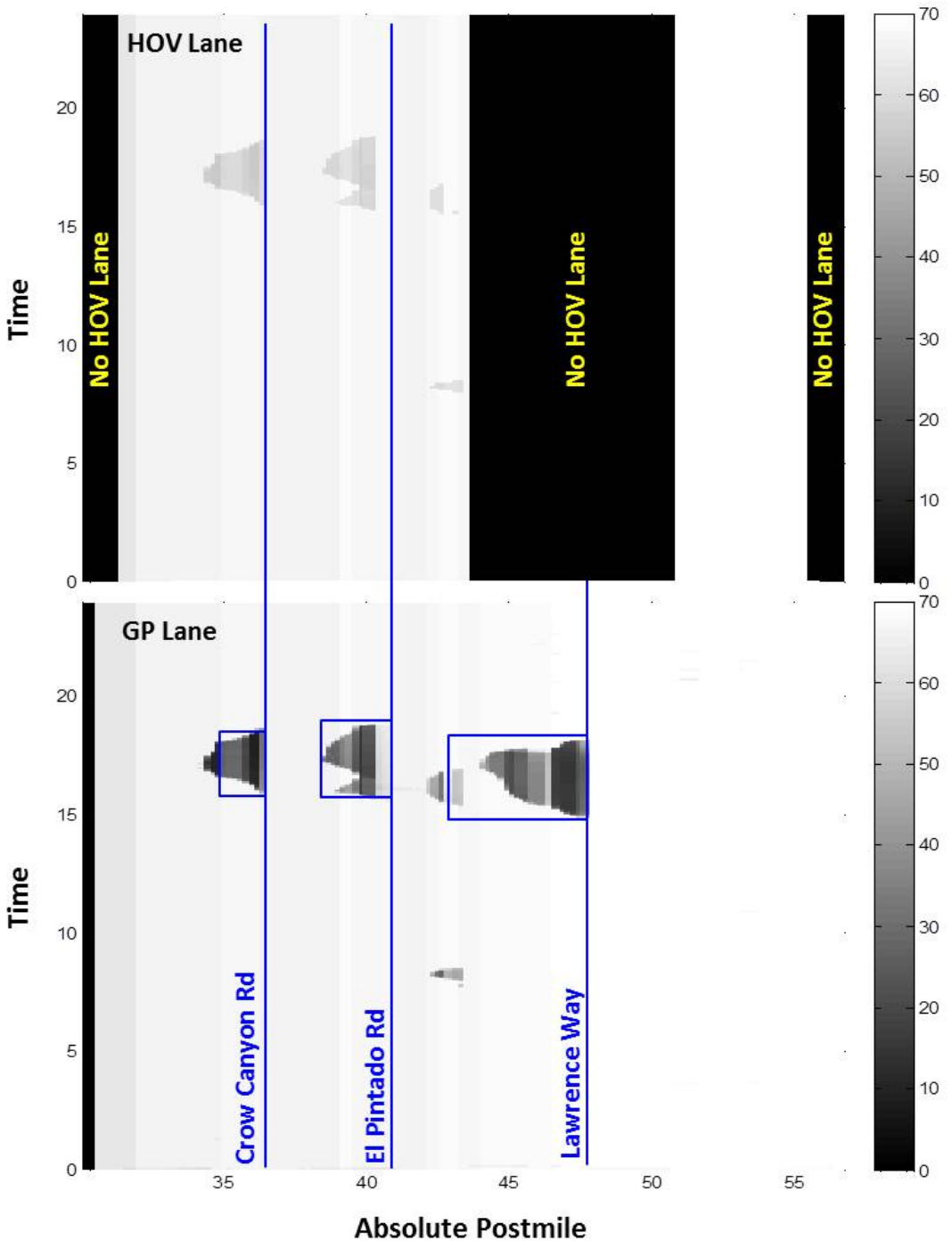

Figure 7: I-680 North speed contours for GP and HOV lanes produced by simulation. Speed values are given in miles per hour. Blue boxes on the GP lane speed contour indicate congested areas as identified by the I-680 CSMP study.

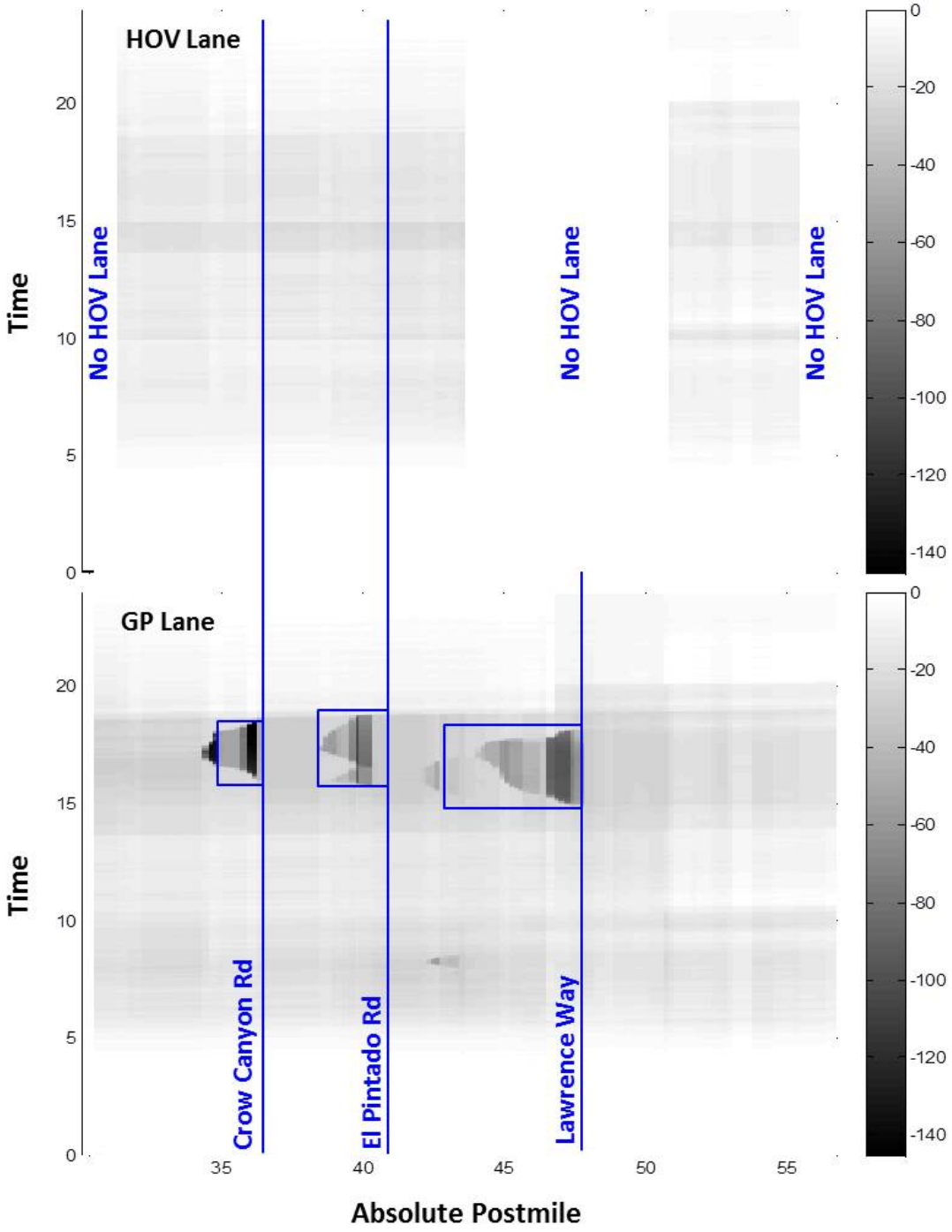

Figure 8: I-680 North density contours for GP and HOV lanes produced by simulation. Density values are given in vehicles per mile per lane. Blue boxes on the GP lane speed contour indicate congested areas as identified by the I-680 CSMP study.

5.2 Gated-Access Managed Lane Case Study: Interstate 210 East

We consider a 20.6-mile stretch of SR-134 East/ I-210 East in Los Angeles County, shown in Figure 11, as a test case for the separated managed lane configuration. This freeway's managed lane is also an HOV lane.

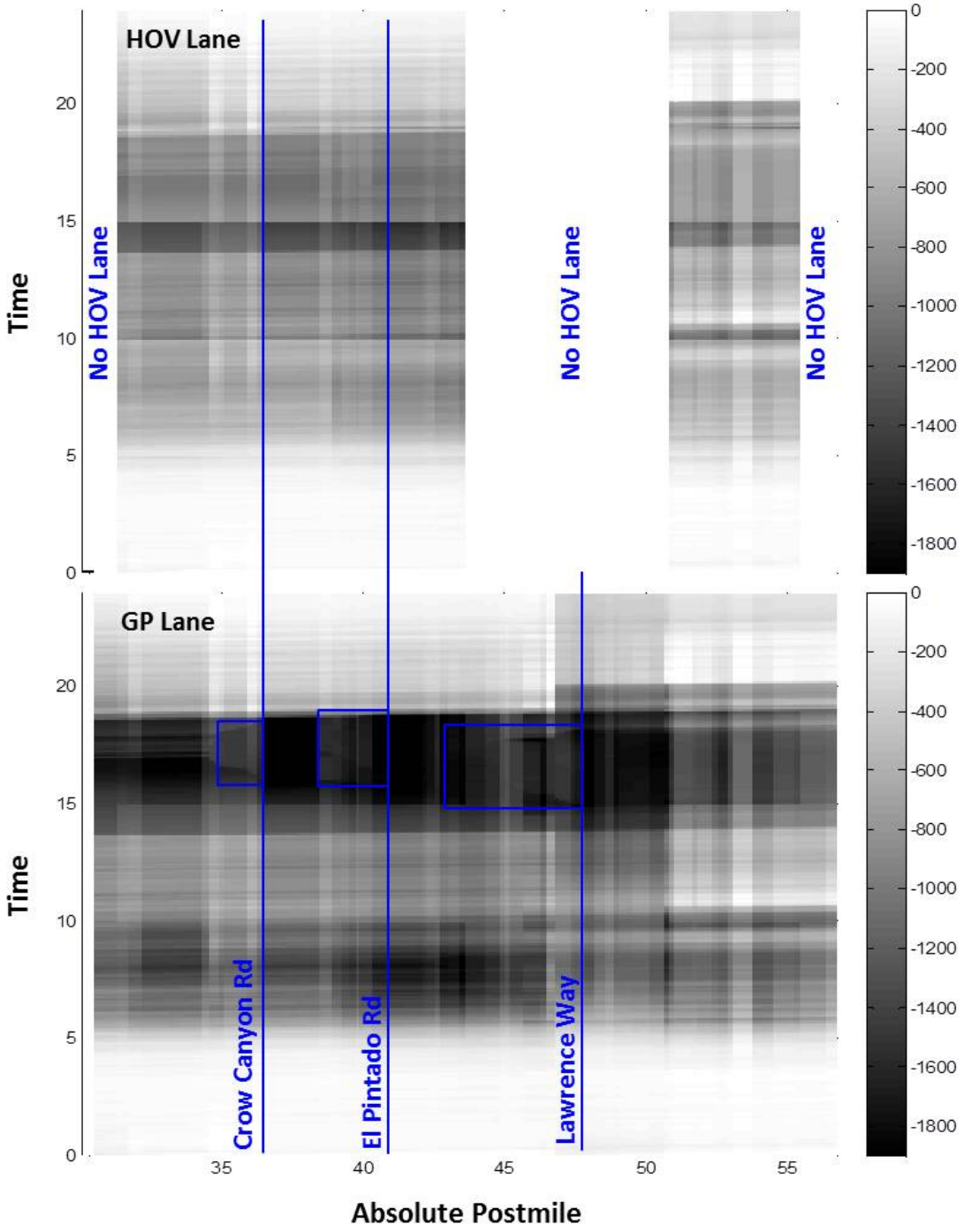

Figure 9: I-680 North flow contours for GP and HOV lanes produced by simulation. Flow values are give in vehicles per hour per lane. Blue boxes on the GP lane speed contour indicate congested areas as identified by the I-680 CSMP study.

This freeway stretch consists of 3.9 miles of SR-134 East from postmile 9.46 to postmile 13.36 and 16.7 miles of I-210 East from postmile 25 to postmile 41.7. Gate locations, where traffic can switch between the GP

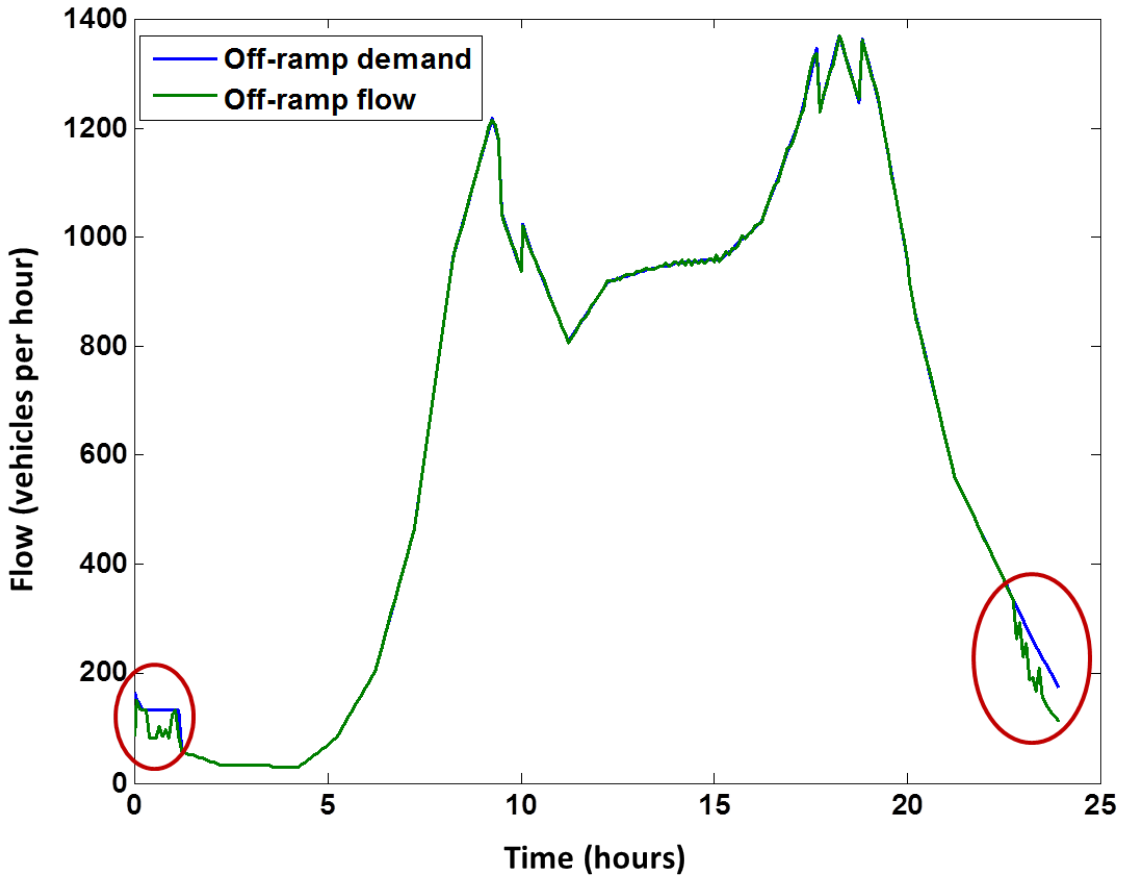

Figure 10: Flow at the Crow Canyon Road off-ramp over 24 hours — collected (off-ramp demand) vs. computed by simulation (off-ramp flow).

	Simulation result	Collected data
GP Lane VMT	1,687,618	-
HOV Lane VMT	206,532	-
Total VMT	1,894,150	1,888,885
GP Lane VHT	27,732	-
HOV Lane VHT	3,051	-
Total VHT	30,783	31,008
GP Lane Delay	2,785	-
HOV Lane Delay	6	-
Total Delay	2,791	2,904

Table 1: Performance measures for I-680 North.

and the HOV lanes are marked on the map. The HOV lane is always active. There are 28 on-ramps and 25 off-ramps. The largest number of off-ramps between two gates is 5. Thus, our freeway model has 7 vehicle classes - LOV, HOV and 5 destination-based.

To build the model, we used PeMS data for the corresponding segments of the SR-134 East and I-210 East for Monday, October 13, 2014 California Department of Tranportation. This was one of the days when most vehicle detectors on the GP and the HOV lanes, on-ramps and off-ramps of SR-134 East and I-210 East

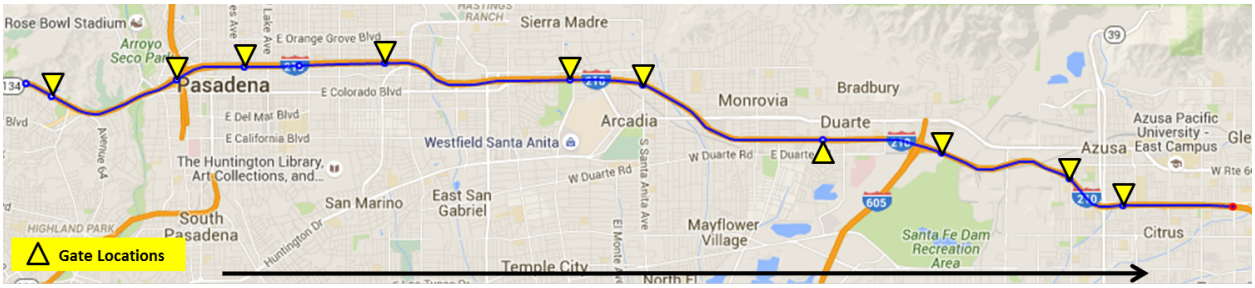

Figure 11: Map of SR-134 East/ I-210 East freeway in Los Angeles County.

were intact, and hence the PeMS data are reliable. Fundamental diagrams were calibrated using PeMS data following the methodology Dervisoglu et al. (2009). As in the I680 North example, we assume that HOV portion of the input demand is 15%.

The modeling results are presented in Figures 12, 13 and 14 showing speed, density and flow contours in the GP and the HOV lanes respectively. Each of these plots consists of the top, corresponding to the HOV lane, and bottom, corresponding to the GP lane, parts. As before, in all the plots traffic moves from left to right along the "Absolute Postmile" axis, while the vertical axis represents time. HOV lane does not get congested. Dashed blue lines on the contour plots indicate HOV gate locations.

Figure 15 shows the PeMS speed contours for the SR-134 East/ I-210 East GP and HOV lanes hat were used as a target for our simulation model. In these plots, traffic also travels from left to right, with the horizontal axis representing postmiles, while the vertical axis represents time. Note that each of the four speed contours has its own color scale (feature of PeMS).

Figure 16 shows an example of how well the off-ramp flow computed by the simulation matches the target, referred to as *off-ramp demand*, taken from the off-ramp at North Hill Avenue. The simulated off-ramp flow matches the off-ramp demand not perfectly, but closely enough. So is the case for all the other off-ramps.

Finally, Table 2 summarizes the performance measurements — VMT, VHT and delay — computed by simulation versus obtained from PeMS. PeMS data come from both SR-134 East and I-210 East, and VMT, VHT and delay values are computed as sums of the corresponding values from these two freeway sections. Delay values are computed in vehicle-hours for those vehicles traveling slower than 45 mph.

	Simulation result	PeMS data
GP Lane VMT	2,017,322	-
HOV Lane VMT	378,485	-
Total VMT	2,395,807	414,941 + 2,006,457 = 2,421,398
GP Lane VHT	33,533	-
HOV Lane VHT	6,064	-
Total VHT	39,597	6,416 + 36,773 = 43,189
GP Lane Delay	3,078	-
HOV Lane Delay	584	-
Total Delay	3,662	1 + 3,802 = 3,803

Table 2: Performance measures for SR-134 East/ I-210 East.

6 Conclusion

In this paper we discussed two managed lane configurations: (1) full access, where special traffic can switch between the GP and the managed lanes at any node; and (2) separated, where special traffic can switch

between the two lanes only at specific nodes, called gates. In the context of the full-access managed lane the *inertia effect* and the *friction effect* were introduced (Section 3.2). The inertia effect reflects drivers' inclination to stay in their lane as long as possible and switch only if this would obviously improve their travel condition. The friction effect reflects the empirically observed drivers' fear of moving fast in the HOV lane while traffic in the adjacent GP links moves slowly due to congestion.

The inertia and, to some extent, friction effect are also present in the separated managed lane. However, the separated managed lane has an additional characteristic: it requires a special modeling trick for sending vehicles traveling in the modeling lane to off-ramps, as locations of gates and off-ramps generally do not coincide. In this paper we proposed such a mechanism. It employs destination based traffic commodities, which are populated at modeling links approaching gates using off-ramp split ratios (Section 3.4). This approach effectively exploits the multi-class feature of our traffic model.

These sorts of traffic network models feature many parameters, and calibrating them can be difficult. We presented an iterative learning approach for estimating some of the harder-to-estimate parameters. Our simulation results comparing our model and calibration results showed good agreement in two case studies, validating both our full-access and gated-access modeling techniques. In the sequel to this paper, we will further extend these results to include control, with simulation of a reactive tolling controller on the managed lane.

Acknowledgement

We would like to express great appreciation to several of our colleagues. To Elena Dorogush and Ajith Muralidharan for sharing ideas, and to Ramtin Pedarsani, Brian Phegley and Pravin Varaiya for their critical reading and their help in clarifying some theoretical issues.

This research was funded by the California Department of Transportation.

A Link Model

For the majority of this paper, we remain agnostic as to the particular functional relationship between occupancy n_l, demand S_l and supply R_l, and flow f_l (also called the fundamental diagram) used in our first-order macroscopic model (2.1). Where a particular fundamental diagram is required, i.e. for the simulation results presented in Section 5 and the example implementation of the friction effect in (3.4), (3.5), (3.6), and (3.7), we use a fundamental diagram from Horowitz et al. (2016). This fundamental diagram captures the oft-observed traffic hysteresis behavior with the "backwards lambda" shape often observed in detector data (Koshi et al., 1983):

$$S_l(t) = v_l^f(t) n_l^c(t) \min\left\{1, \frac{F_l(t)}{v_l^f(t)\sum_{c=1}^{C} n_l^c(t)}\right\}, \tag{A.1}$$

$$R_l(t) = (1-\theta_l(t))\, F_l(t) + \theta_l(t) w_l(t)\left(n_l^J(t) - \sum_{c=1}^{C} n_l^c(t)\right), \tag{A.2}$$

where, for link l, F_l is the capacity, v_l^f is the freeflow speed, w_l is the congestion wave speed, n_l^J is the jam occupancy, and $n_l^- = \frac{w_l n_l^J}{v_l^f + w_l}$ and $n_l^+ = \frac{F_l}{v_l^f}$ are called the *low* and *high critical occupancies*, respectively. The variable $\theta_l(t)$ is a congestion metastate of l, which encodes the hysteresis:

$$\theta_l(t) = \begin{cases} 0 & n_l(t) \le n_l^-, \\ 1 & n_l(t) > n_l^+, \\ \theta_l(t-1) & n_l^- < n_l(t) \le n_l^+. \end{cases} \tag{A.3}$$

Examining (A.3) and (A.2), we see that when a link's occupancy goes above n_l^+ (i.e., when it becomes congested), its ability to receive flow is reduced until the occupancy falls below n_l^-.

An image of (A.1) and (A.2) overlaid on each other, giving a schematic image of the fundamental diagram, is shown in Fig. 17. Unless $n_l^- = n_l^+$, when it assumes triangular shape, the fundamental diagram is not a function of occupancy alone (i.e., without $\theta_l(t)$): $n_l(t) \in \left(n_l^-, n_l^+\right]$ admits two possible flow values.

References

California Department of Tranportation. PeMS homepage. `http://pems.dot.ca.gov`.

M. J. Cassidy, K. Kim, W. Ni, and W. Gu. A problem of limited-access special lanes. Part I: Spatiotemporal studies of real freeway traffic. *Transportation Research Part A: Policy and Practice*, 80:307 – 319, 2015. ISSN 0965-8564. doi: http://dx.doi.org/10.1016/j.tra.2015.07.001. URL `http://www.sciencedirect.com/science/article/pii/S0965856415001834`.

M. Chang, J. Wiegmann, A. Smith, and C. Bilotto. A Review of HOV Lane Performance and Policy Options in the United States. Report FHWA-HOP-09-029, Federal Highway Administration, 2008.

C. F. Daganzo. A behavioral theory of multi-lane traffic flow. Part i: Long homogeneous freeway sections. *Transportation Research Part B: Methodological*, 36(2):131 – 158, 2002. ISSN 0191-2615. doi: http://dx.doi.org/10.1016/S0191-2615(00)00042-4. URL `http://www.sciencedirect.com/science/article/pii/S0191261500000424`.

C. F. Daganzo and M. J. Cassidy. Effects of high occupancy vehicle lanes on freeway congestion. *Transportation Research Part B: Methodological*, 42(10):861–872, Dec. 2008. ISSN 01912615. doi: 10.1016/j.trb.2008.03.002. URL `http://linkinghub.elsevier.com/retrieve/pii/S0191261508000325`.

G. Dervisoglu, G. Gomes, J. Kwon, A. Muralidharan, P. Varaiya, and R. Horowitz. Automatic calibration of the fundamental diagram and empirical obsevations on capacity. *88th Annual Meeting of the Transportation Research Board, Washington, D.C., USA*, 2009.

N. Farhi, H. Haj-Salem, M. Khoshyaran, J.-P. Lebacque, F. Salvarani, B. Schnetzler, and F. De Vuyst. The Logit lane assignment model: first results. In *TRB 92nd Annual Meeting Compendium of Papers*, 2013.

S. Hoogendoorn and P. Bovy. Gas-Kinetic Model for Multilane Heterogeneous Traffic Flow. *Transportation Research Record: Journal of the Transportation Research Board*, 1678:150–159, 1999. doi: 10.3141/1678-19.

S. P. Hoogendoorn and P. H. Bovy. Continuum modeling of multiclass traffic flow. *Transportation Research Part B: Methodological*, 34(2):123 – 146, 2000. ISSN 0191-2615. doi: http://dx.doi.org/10.1016/S0191-2615(99)00017-X. URL `http://www.sciencedirect.com/science/article/pii/S019126159900017X`.

R. Horowitz, A. A. Kurzhanskiy, A. Siddiqui, and M. A. Wright. Modeling and control of hot lanes. Technical report, Partners for Advanced Transportation Technologies, University of California, Berkeley, Berkeley, CA, 2016.

K. Jang and M. Cassidy. Dual influences on vehicle speed in special-use lanes and critique of US regulation. *Transportation Research, Part A*, 46(2012):1108–1123, 2012.

K. Jang, S. Oum, and C.-Y. Chan. Traffic Characteristics of High-Occupancy Vehicle Facilities: Comparison of Contiguous and Buffer-Separated Lanes. *Transportation Research Record: Journal of the Transportation Research Board*, 2278:180–193, 2012. doi: 10.3141/2278-20.

M. Koshi, M. Iwasaki, and I. Ohkura. Some findings and an overview on vehicular flow characteristics. In *Proceedings of the 8th International Symposium on Transportation and Traffic Flow Theory*, volume 198, pages 403–426, 1983.

A. A. Kurzhanskiy and P. Varaiya. Traffic management: An outlook. *Economics of Transportation*, 4(3): 135–146, Sept. 2015. ISSN 22120122. doi: 10.1016/j.ecotra.2015.03.002.

X. Liu, B. Schroeder, T. Thomson, Y. Wang, N. Rouphail, and Y. Yin. Analysis of operational interactions between freeway managed lanes and parallel, general purpose lanes. *Transportation Research Record: Journal of the Transportation Research Board*, 2262:62–73, 2011.

X. Liu, G. Zhang, Y. Lao, and Y. Wang. Modeling Traffic Flow Dynamics on Managed Lane Facility: Approach Based on Cell Transmission Model. *Transportation Research Record: Journal of the Transportation Research Board*, 2278:163–170, 2012.

T. Lomax, D. Schrank, and B. Eisele. The 2015 Annual Urban Mobility Scorecard. Technical report, Texas Transportation Institute, 2015. `http://mobility.tamu.edu`.

D. McFadden. Conditional Logit Analysis of Qualitative Choice Behavior. In P. Zarembka, editor, *Frontiers in Econometrics*, pages 105–142. Academic Press, New York, 1973.

D. Ngoduy. *Macroscopic discontinuity modeling for multiclass multilane traffic flow operations*. PhD thesis, Delft University of Technology, 2006.

J. Obenberger. Managed lanes: Combining access control, vehicle eligibility, and pricing strategies can help mitigate congestion and improve mobility on the nationâĂŹs busiest roadways. *Public Roads*, 68(3):48–55, 2004. URL `http://www.fhwa.dot.gov/publications/publicroads/04nov/08.cfm`.

Y. Shiomi, T. Taniguchi, N. Uno, H. Shimamoto, and T. Nakamura. Multilane first-order traffic flow model with endogenous representation of lane-flow equilibrium. *Transportation Research Part C: Emerging Technologies*, In press:–, 2015. ISSN 0968-090X. doi: http://dx.doi.org/10.1016/j.trc.2015.07.002.

M. Treiber, A. Hennecke, and D. Helbing. Derivation, properties, and simulation of a gas-kinetic-based, nonlocal traffic model. *Phys. Rev. E*, 59:239–253, Jan 1999. doi: 10.1103/PhysRevE.59.239. URL `http://link.aps.org/doi/10.1103/PhysRevE.59.239`.

J. van Lint, S. Hoogendoorn, and M. Schreuder. Fastlane: New Multiclass First-Order Traffic Flow Model. *Transportation Research Record: Journal of the Transportation Research Board*, 2088:177–187, 2008. doi: 10.3141/2088-19.

G. Wong and S. Wong. A multi-class traffic flow model - an extension of LWR model with heterogeneous drivers. *Transportation Research Part A: Policy and Practice*, 36(9):827 – 841, 2002. ISSN 0965-8564. doi: http://dx.doi.org/10.1016/S0965-8564(01)00042-8. URL `http://www.sciencedirect.com/science/article/pii/S0965856401000428`.

M. A. Wright, G. Gomes, R. Horowitz, and A. A. Kurzhanskiy. On node and route choice models for high-dimensional road networks. *Submitted to Transportation Research Part B*, 2016a.

M. A. Wright, R. Horowitz, and A. A. Kurzhanskiy. A dynamic system characterization of road network node models. In *Proceedings of the 10th IFAC Symposium on Nonlinear Control Systems*, August 2016b.

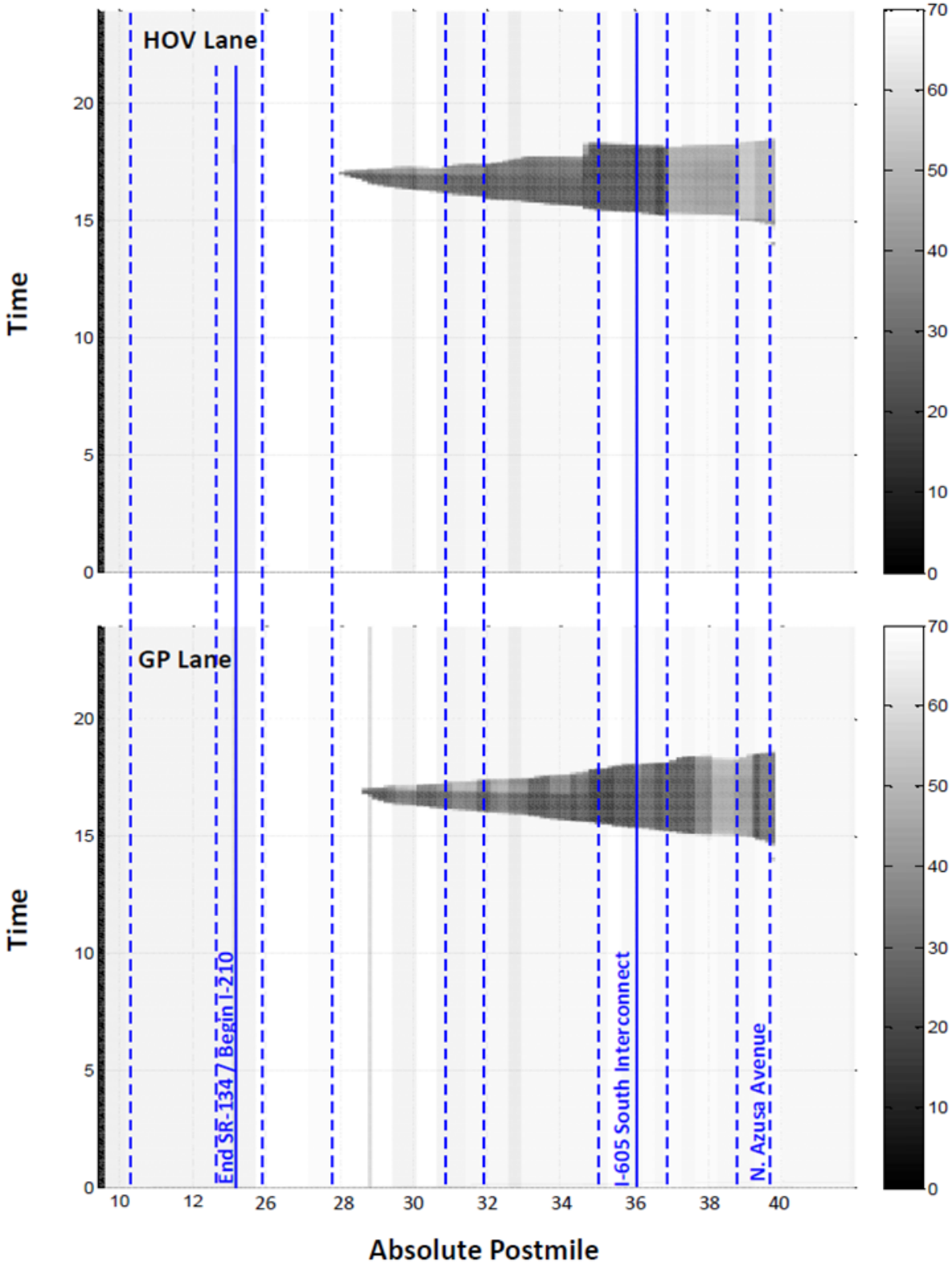

Figure 12: SR-134 East/ I-210 East speed contours for GP and HOV lanes produced by simulation. Speed values are given in miles per hour.

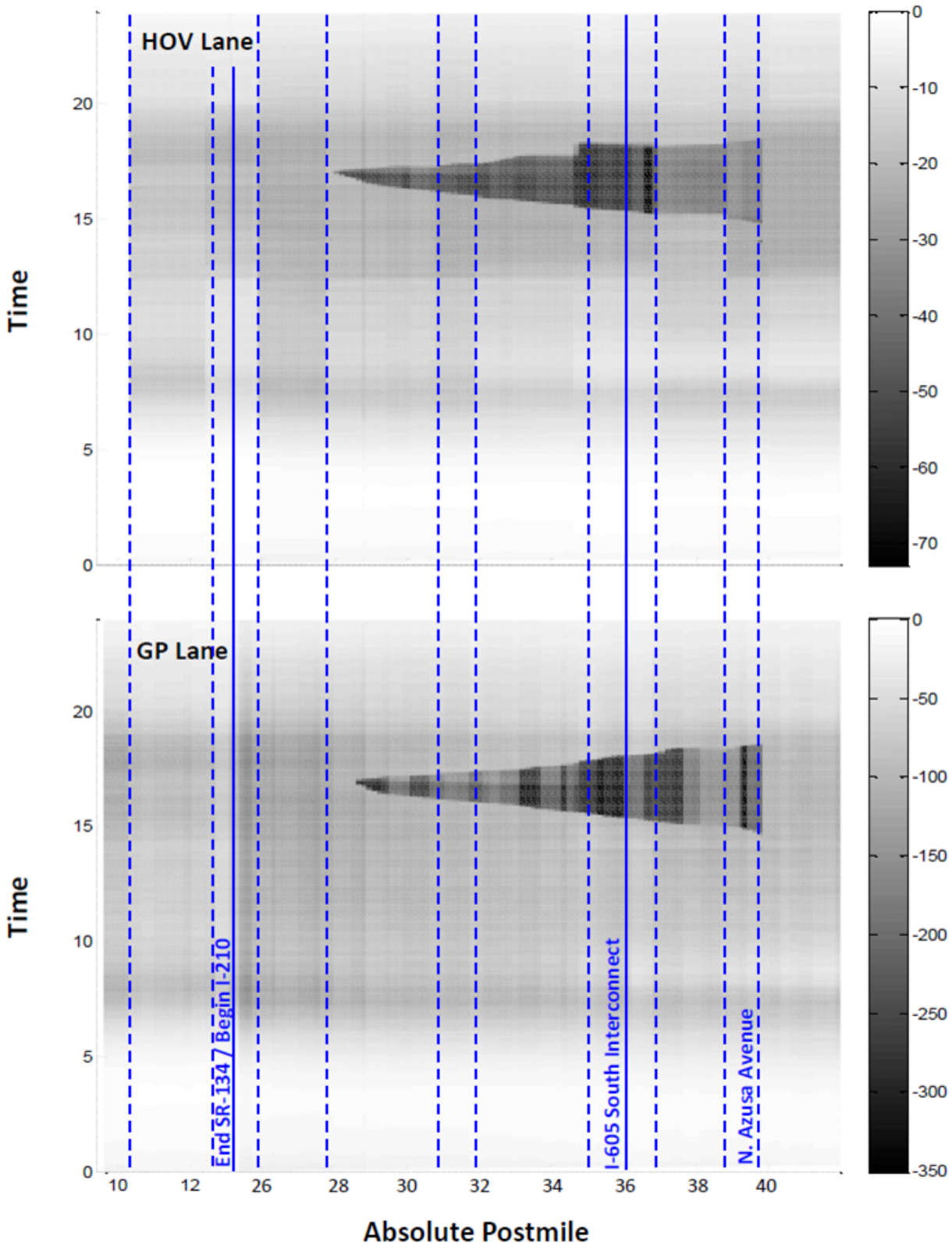

Figure 13: SR-134 East/ I-210 East density contours for GP and HOV lanes produced by simulation. Density values are given in vehicles per mile per lane.

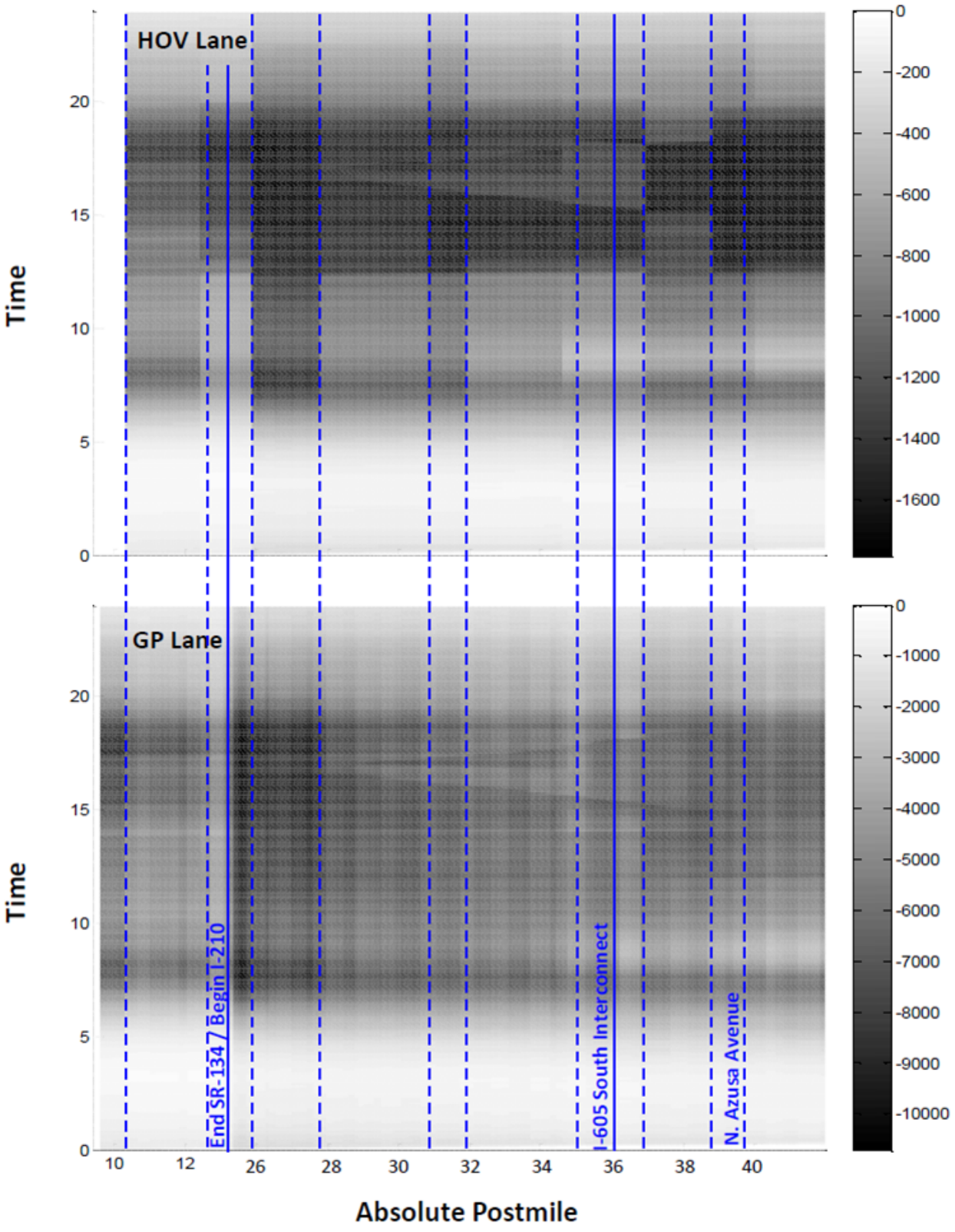

Figure 14: SR-134 East/ I-210 East flow contours for GP and HOV lanes produced by simulation. Flow values are give in vehicles per hour per lane.

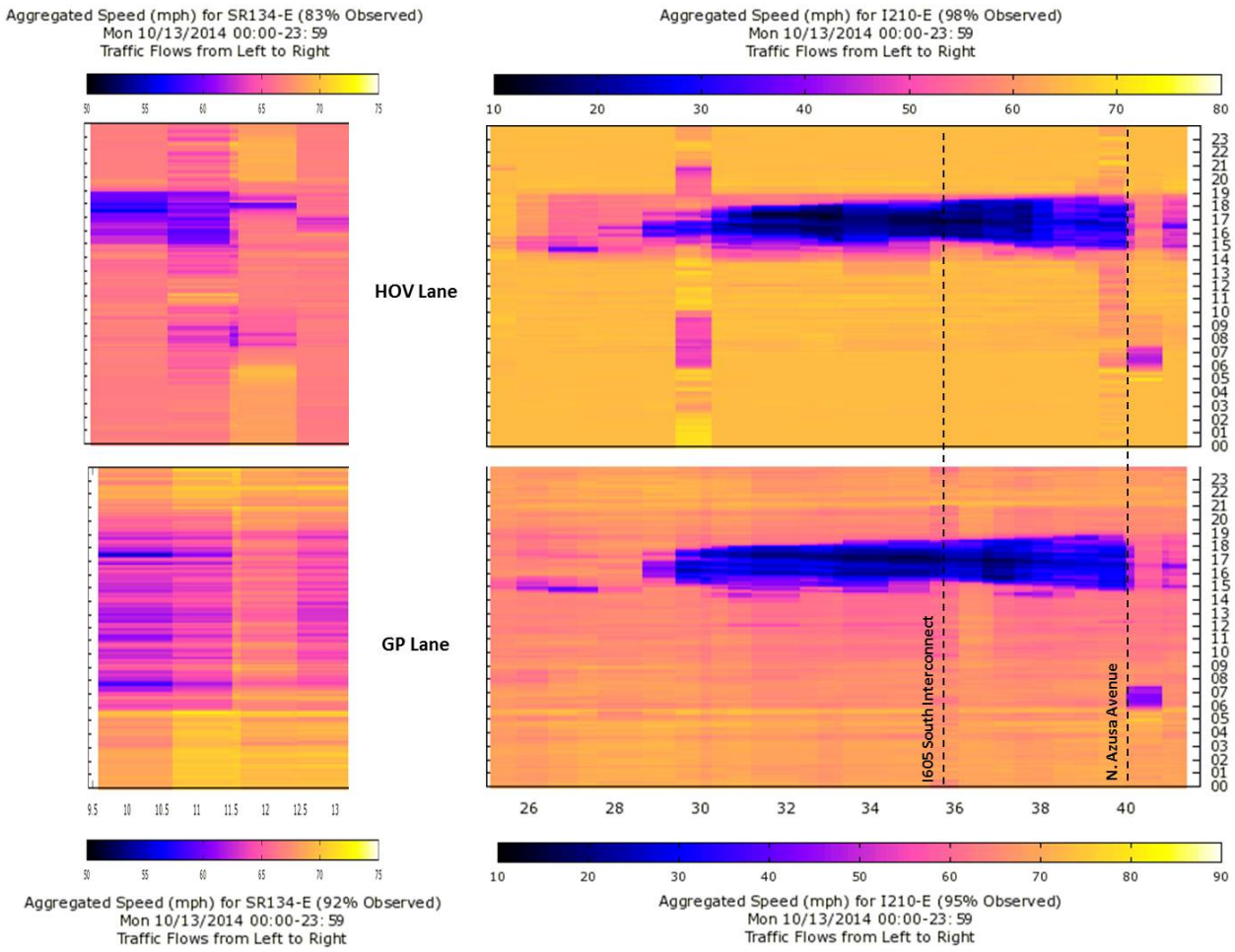
Aggregated Speed (mph) for SR134-E (83% Observed)
Mon 10/13/2014 00:00-23:59
Traffic Flows from Left to Right
Aggregated Speed (mph) for I210-E (98% Observed)
Mon 10/13/2014 00:00-23:59
Traffic Flows from Left to Right
HOV Lane
GP Lane
I605 South Interconnect
N. Azusa Avenue
Aggregated Speed (mph) for SR134-E (92% Observed)
Mon 10/13/2014 00:00-23:59
Traffic Flows from Left to Right
Aggregated Speed (mph) for I210-E (95% Observed)
Mon 10/13/2014 00:00-23:59
Traffic Flows from Left to Right

Figure 15: SR-134 East/ I-210 East speed contours for GP and HOV lanes obtained from PeMS California Department of Tranportation for Monday, October 13, 2014. Horizontal axis represents Absolute postmile, and vertical axis represents time in hours.

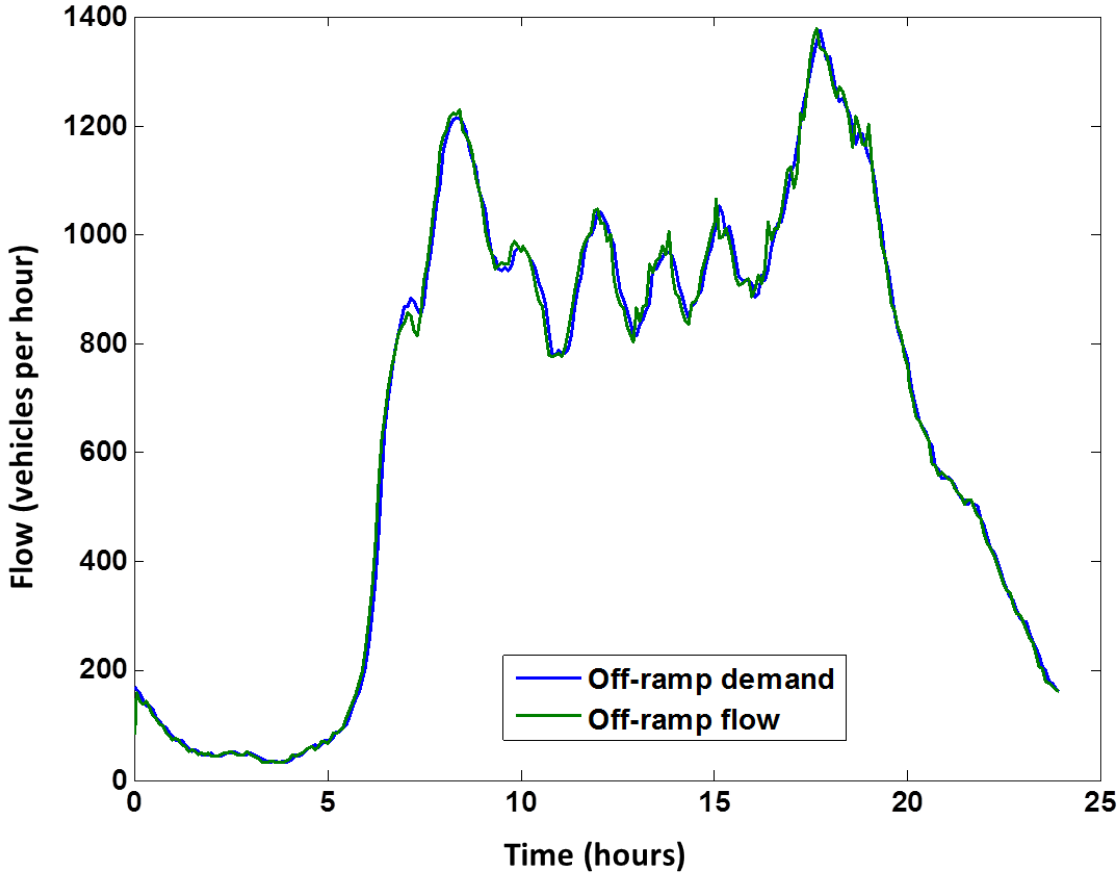

Figure 16: Flow at the North Hill Avenue off-ramp over 24 hours — PeMS data (off-ramp demand) vs. computed by simulation (off-ramp flow).

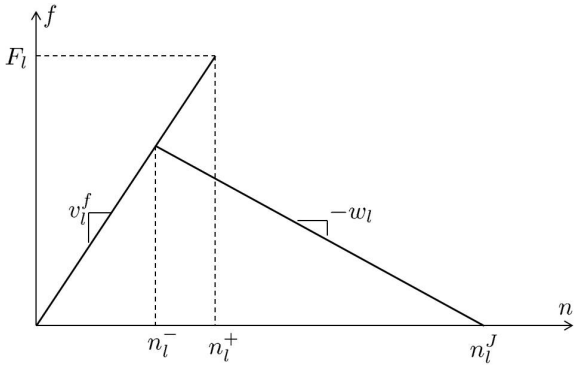

Figure 17: The "backwards lambda" fundamental diagram.